Chapter 4

Results and Discussion

This chapter discusses a number of results obtained from our Timing Observations. In the section 4.1, we present and discuss the average profiles obtained for all the pulsars and give the rotational, derived and the improved positional parameters obtained from Timing Analysis. This is followed by the discussion of the effect of scattering due to interstellar medium on the observed pulses in section 4.2 and we also present the scatter broadening measurements on 10 pulsars in this section. In the section 4.3 we present a brief **discussion** of re-analysis of pulsar current and birth rate after including contributions from our samples and the latest **Parkes** Survey. In the section 4.4 we discuss the peculiar motion of PSR **1952+29** and possibility of it having a binary companion based on our and earlier data.

4.1 Results of Timing Analysis

4.1.1 Average profiles of 16 pulsars

The **integrated/average** pulse profile of any **pulsar** obtained by averaging a few hundreds to thousands of pulses shows remarkable stability in **contrast** to pulse-to-pulse variations. Rankin(1983a,b,1986,1990,1993) and Lyne & **Manchester(1988)** have **done** a detailed classification of pulsars based on their pulse shape and polarisation characteristics. It is believed that there are two basic kinds of emission components present, namely a core emission and a hollow **conal** emission, which gives rise to a **core(central)** componeet and one or more pairs of conal pair components (wings) respectively, Depending upon how the line-of-sight cuts **across** the emission beam, one would get a single/double/triple/quadruple or multiple components,' Observations show that the central core.component emitted relatively **close** to the surface, has antisymmetric circular **polarisation** variation in longitude and a relatively steep intensity spectrum. But the hollow conical beam is **radiated** at a height of $\sim 10^8$ cm. Also, it has a relatively flat spectrum and displays an S-shaped traverse of the position angle of linear polarisation. Hence, polarisation studies are important in order to **classify** the profiles **as** whether they belong to conal or core emission. In the present case, however, the telescope we have used can detect only single linear polarisation, so the polarisation characteristics could not be studied. Nevertheless, one could make use of the empirical relation of core widths to the period (Rankin 1993),

$$W_{\text{core}} = 2^{\circ}.45P^{-0.5}/\sin(\alpha) \tag{4.1}$$

where W_{core} is the observed width of the core component, P is the period of the pulsar and α is the angle between the rotation axis and the magnetic axis. From this, one would be able to calculate the minimum width expected by assuming α to be 90°. If the measured width of the pulse component is less than the expected, then one can rule out with confidence the possibility of the observed component being a core component and hence it can be interpreted as a conal component. Here, of course, one has assumed that the polarisation vector does not rotate faster than the total intensity variation which may not be true in all cases. We have attempted to classify our sample of pulsars on these lines.

The average profiles of all the 16 pulsars in our sample is shown in fig 4.1 & fig 4.2. Each profile is an average of about 30 runs of 10 minute each.

- ***PSR J0134-2937***
  The duty cycle of this pulsar is $\sim 5\%$ at 327 MHz. The measured pulse width is 6.4 ms and if extrapolated to 1 GHz using the power law dependence of $f^{-0.25}$ (Rankin 1983b), it turns out to be greater than the expected minimum width of core ($W_{\text{core}}^{\text{min}}$) of 2.5 ms for this period. So, one would conclude that the main pulse could be a core component but one sees a possible suggestion of one more component 17 mP away from the main one, with a relative strength of ~ 0.45. As the half-triple profiles (one core and one cone component) are relatively rare, the possible presence of the second component makes the profile more likely of a conal double type.

- ***PSR J0459-0210***
  This pulsar shows definitely the existence of two components. The pulse width of the main component is 22 ms at 327 MHz and it seems to be more than the $W_{\text{core}}^{\text{min}}$ at 1 GHz. The second component has a relative strength of 0.36. It is more likely that both the components are conal components.

- ***PSR J1034-3224***
  This pulsar appears to be a classic example for complex M-type profile, having definitely three or four components spread over $\sim 75^{\circ}$ of longitude. The width of the strongest component is found to be 23 ms. The second, third and the fourth components have relative strengths of 0.3, 0.15 and 0.22 respectively. The second component could be a core component, but if not, this would be an example of a Conal Quadruple(cQ).

- ***PSR J1141-3310***
  This pulsar also shows the possible existence of a second component with a relative

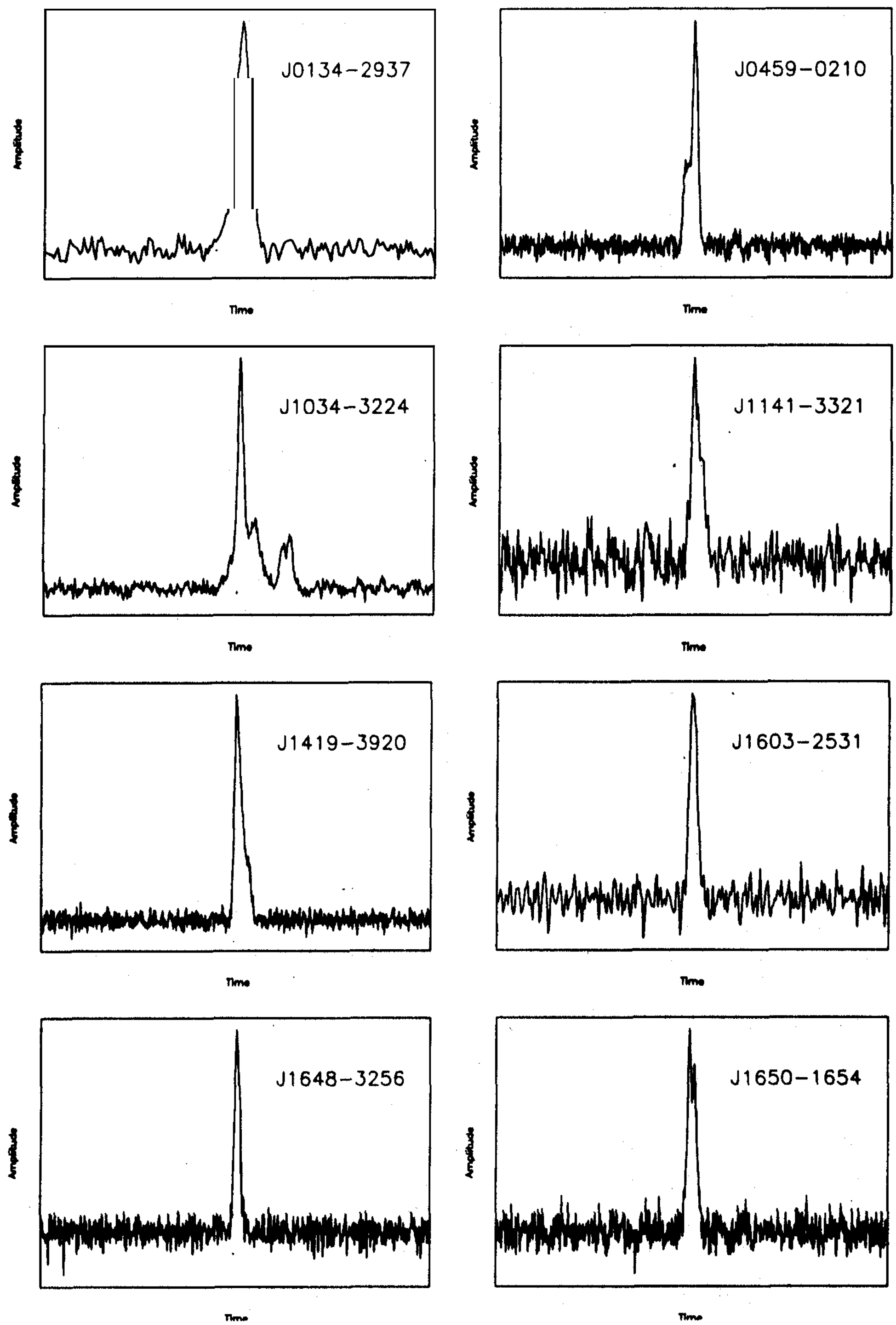

Figure 4.1: The integrated profiles of the 16 pulsars observed at 327 MHz is given in two pages. Each profile is over the corresponding pulsar period.

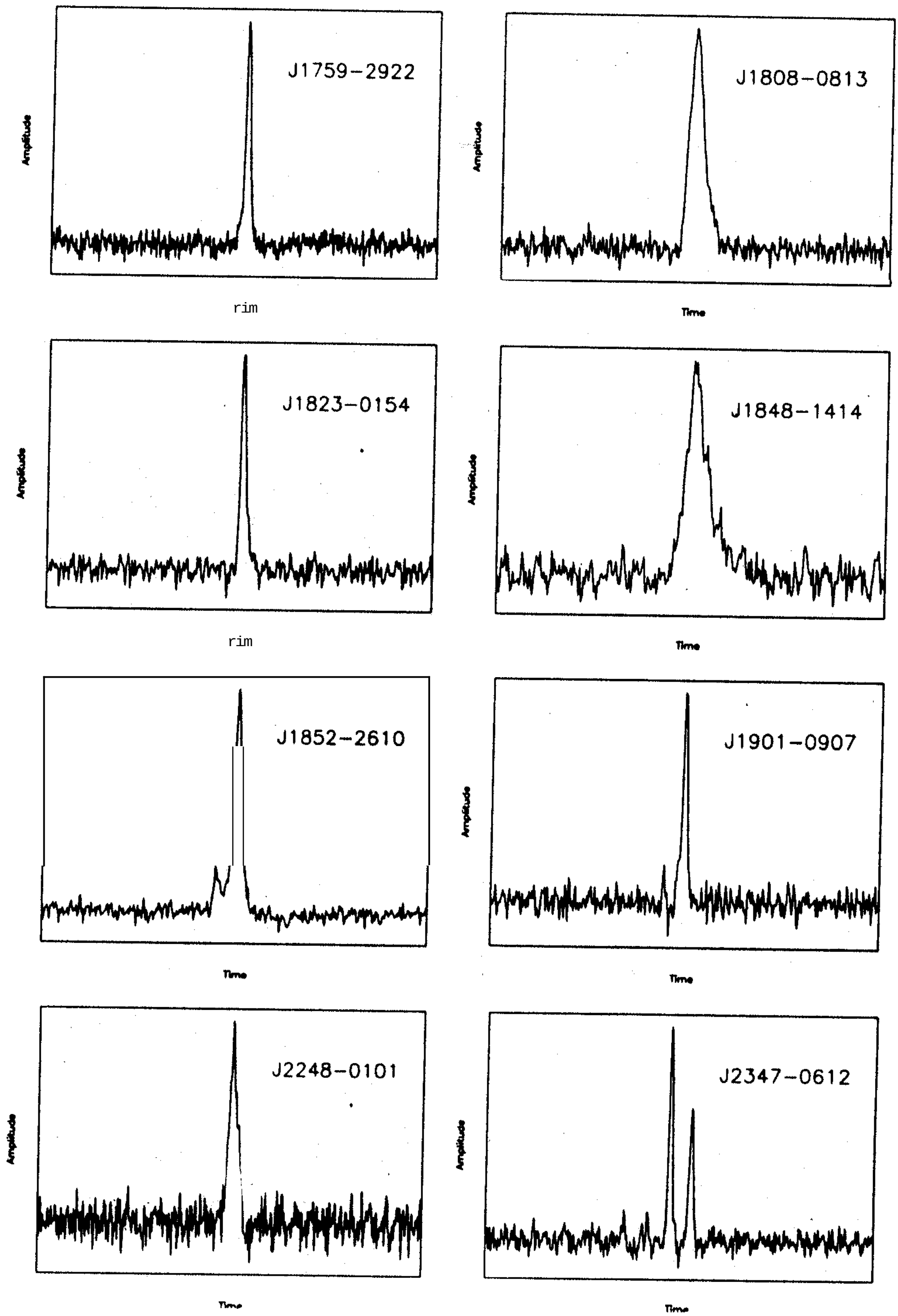

Figure 4.2: Integrated profiles continued from the last page

height of 0.5 and at a separation of 20 mP from the main component. The total pulse width is about 5 ms while the width of the main component is 3.3 ms, which is close to the W_{core}^{min} at 1 GHz.

- ***PSR J1419-3920***
  The total pulse width is 25.8ms at 327 MHz and there is a possibility of a second component $\sim$ 27 mP away from the main component with a relative strength of 0.25. The W_{core}^{min} is ~7 ms (at 1GHz) which is much smaller than the observed width extrapolated to 1GHz.

- ***PSR J1603-2531***
  This pulsar has only one component of width of 7 ms at 327 MHz and the extrapolated width at 1GHz is 5.8 ms which is greater than the W_{core}^{min} for this period. Given also that the profile is somewhat symmetric, it is more likely that this component is the core component.

- ***PSR J1648-3256***
  A very narrow pulse with a duty cycle of 1.7% is observed for this pulsar, but it is still larger than that expected for the minimum width of the core component. It is tempting to consider this as a core component.

- ***PSR J1650-1654***
  This pulsar shows a bifurcation near the top of the pulse, indicating that there are two components, but given the amount of noise this is somewhat uncertain. The duty cycle of this pulsar is 4.5% and the total half power width is 45.6 ms. This pulsar may be an example of the conal double class, if there are indeed two components.

- ***PSR J1759-2922***
  The profile is consistent with a single component of width 9.3 ms. The width extrapolated to 1 GHz is 7 ms which is greater than the W_{core}^{min}. Hence, we would classify this as a core single type.

- ***PSR J1808-0813***
  This pulsar has a noticeable scattering tail of width 18 ms and its intrinsic pulse width is estimated to be ~30 ms. This intrinsic width is much more than the W_{core}^{min}, and in addition, a single intrinsic component model fits the data better (ref. Section 4.2). Considering these, we tentatively identify this as a core component.

- ***PSR J1823-0154***
  This pulsar also has a scattering tail of width $\sim$5 ms and the intrinsic pulse width seems to be $\sim$9 ms and it is close to the W_{core}^{min} at 1GHz. So if it is the core component then the inclination of the field axis would be nearly orthogonal to the rotation axis. It is important to note however that the total observed width at 327 MHz is significantly less than the width of 15 ms at 436 MHz quoted in the Catalogue.

- ***PSR J1848-1414***
  The estimated intrinsic width of the pulse is **13.5** ms and the scattering tail width is measured to be **-9.5** ms. The intrinsic width extrapolated to 1GHz is greater than the W_{core}^{min}. Although the pulse is quite broadened because of the scattering which spreads over $\sim 90°$ of longitude, the modelling in section 4.2 favours only a single component which is possibly a core component.

- ***PSR J1852-2610***
  This pulsar clearly shows two components with a separation of **55 mP.** The width of the main pulse is measured to be **-9 ms** and the second component is quite weak having a relative strength of only –0.2. The width of the strongest component at 1GHz seems to be greater than the expected minimum width for the core component for this period. However, tentatively one would classify this profile as a conal double.

- ***PSR J1901-0907***
  This pulsar has a very narrow pulse width of **14.5** ms and a corresponding duty cycle of **1.6%.** There is a hint of an unresolved component on the rising edge of the main component. Also, it looks like there is a second component but it's of spiky nature. If the weaker components indeed exist, then this profile would be classified as a triple.

- ***PSR J2248-0101***
  This pulsar has a pulse width of –17 ms, and may have two components with a separation of $\sim$ **16 mP.** The pulse width extrapolated to 1GHz is greater than the expected core width. However, in the light of the possible two components the profile would more likely be a conal double.

- ***PSR J2347-0612***
  This pulsar has a clear double profile showing an example of a conal double. The component separation is 54 mP. The width of the stronger component is **-16 ms** and that of the second component is **-13 ms.** The relative strength of the second component is **0.65.**

4.1.2 Rotational and Derived parameters

Using the analysis procedure described in chapter 3, we have obtained the phase residuals for each pulsar. An example of the raw (unfitted) phase residuals is shown in fig(4.3a). The randomness seen in the phase residuals is due to the large error in the period (a few parts in a million) of the pulsar, the absence of the period derivative estimate and relatively large possible errors (of the order of a few arcminutes) in the assumed positions of the pulsar. Hence, a combined fit for P, $\dot{P}$ and position is not possible. In order to obtain an initial estimate for position and period derivative, we did the following: we estimated the period over small epoch ranges using a first-order fit to the preliminary phase residuals as shown in fig(4.4a). Then we did a least-square fit for P and for error in positions (Aa, AS) using the following equation of P,

$$P = P_o + \dot{P}(t - t_o) + P\left[\Delta\alpha\frac{dA}{dt} + \Delta\delta\frac{dB}{dt}\right] \tag{4.2}$$

where P_o is the period at t_o, A and B are defined in equation (3.15). The fitted period residuals are shown in **fig(4.4b)**. It is worth pointing out that the period residuals computed this way are considerably less sensitive to the possible phase wraps due to large uncertainties in the assumed initial **parameters.**

Using these initial estimates, the phase residuals were re-estimated and the **bootstrap**ping method was applied on the phase residuals to obtain the improved values of P, P and position. As seen from **eqn.(3.14)**, the position offsets are modelled with only the lowest order terms. It is important to repeat the procedure (starting with re-estimation of the phase residuals with successively improved initial estimates) a few times till convergence is obtained. To illustrate the phase residual behaviour, we **have** shown an example in **fig(4.3b)** of how the phase residuals vary when there is an error in the period derivative and when there is an error in the position in **fig(4.3c)**. The final residuals are shown in fig(4.5) for all the pulsars.

Once the rotational parameters are known, we can derive a few other parameters such as surface magnetic field (B) and the characteristic age (τ_{ch}) for a given pulsar using the following equations,

$$B = 3.2 \times 10^{19}(P\dot{P})^{\frac{1}{2}} \quad G \tag{4.3}$$

$$\tau_{ch} = \frac{P}{2\dot{P}} \quad sec \tag{4.4}$$

where P is in **sec** and $\dot{P}$ is in units of ss^{-1}.

The best-fit rotational parameters obtained from the arrival time analysis and the derived parameters calculated using our new estimates of P, P for the present sample are listed in Table (4.1). The periods (P) and the period derivatives ($\dot{P}$) are quoted for a reference epoch chosen near the starting time of the data span. For all these pulsars, the period uncertainties (after the second-order fit) are improved to a part in 10^{11} compared to $\sim$ 1 part in 10^5 (as given in the catalogue). The period derivatives for all the pulsars in our list have been obtained for the first time.

Fig(4.6) shows the location of pulsars in our sample in $\log(\dot{P})$ - $\log(P)$ diagram. 11 of the 16 pulsars in our sample fall within the main island of the normal pulsars, while 4 pulsars definitely stand out considering the implied values of the magnetic field. A possible population of recycled pulsars in the field range of $10^{10.5}$ to $10^{11.5}$ G was identified by Deshpande, **Ramachandran** & **Srinivasan** (1995). The above mentioned 4 pulsars would belong to this population. Given that only $\sim$**11%** of the observed pulsar population is found to have fields $10^{10.5} < B < 10^{11.5}$, it is interesting that 25% of our sample chosen with no explicit bias falls in this range. Although statistically this may not be very significant, it definitely illustrates the kind of bias that may exist in the distribution of pulsars for which P values are yet to be determined. It is interesting also to note that

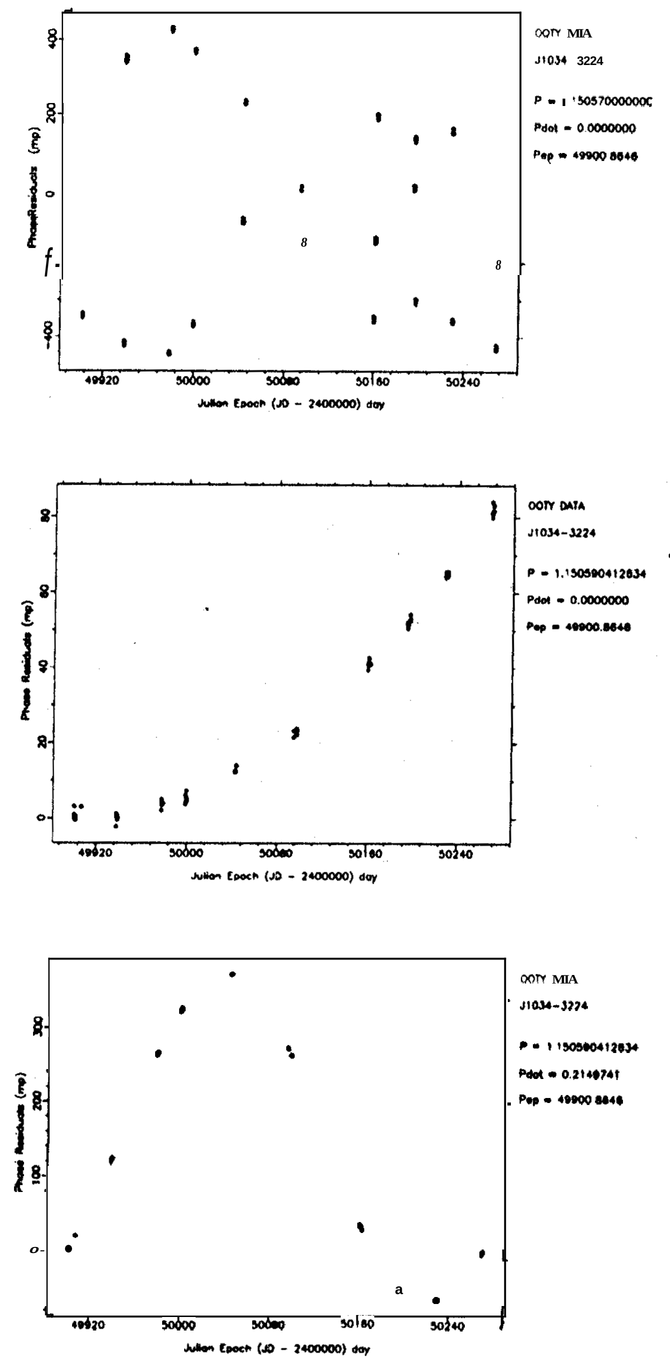

Figure 4.3: Phase residuals of PSR **J1034-3224.** The top figure shows the raw phase residuals which **are** obtained from the existing catalogue period and position. The middle figure shows the quadratic variation of phase residuals when $\dot{P}$ is not accounted for. The last figure shows the sinusoidal variation of phase **residuals** due to positional error while $\dot{P}$ is taken care of. Here in the legend P is in sees, Pdot represents the period derivative in 10^{-15} ss^{-1} and Pep represents the reference epoch in Truncated Julian days (JD-2400000) for the period and the period derivative value given.

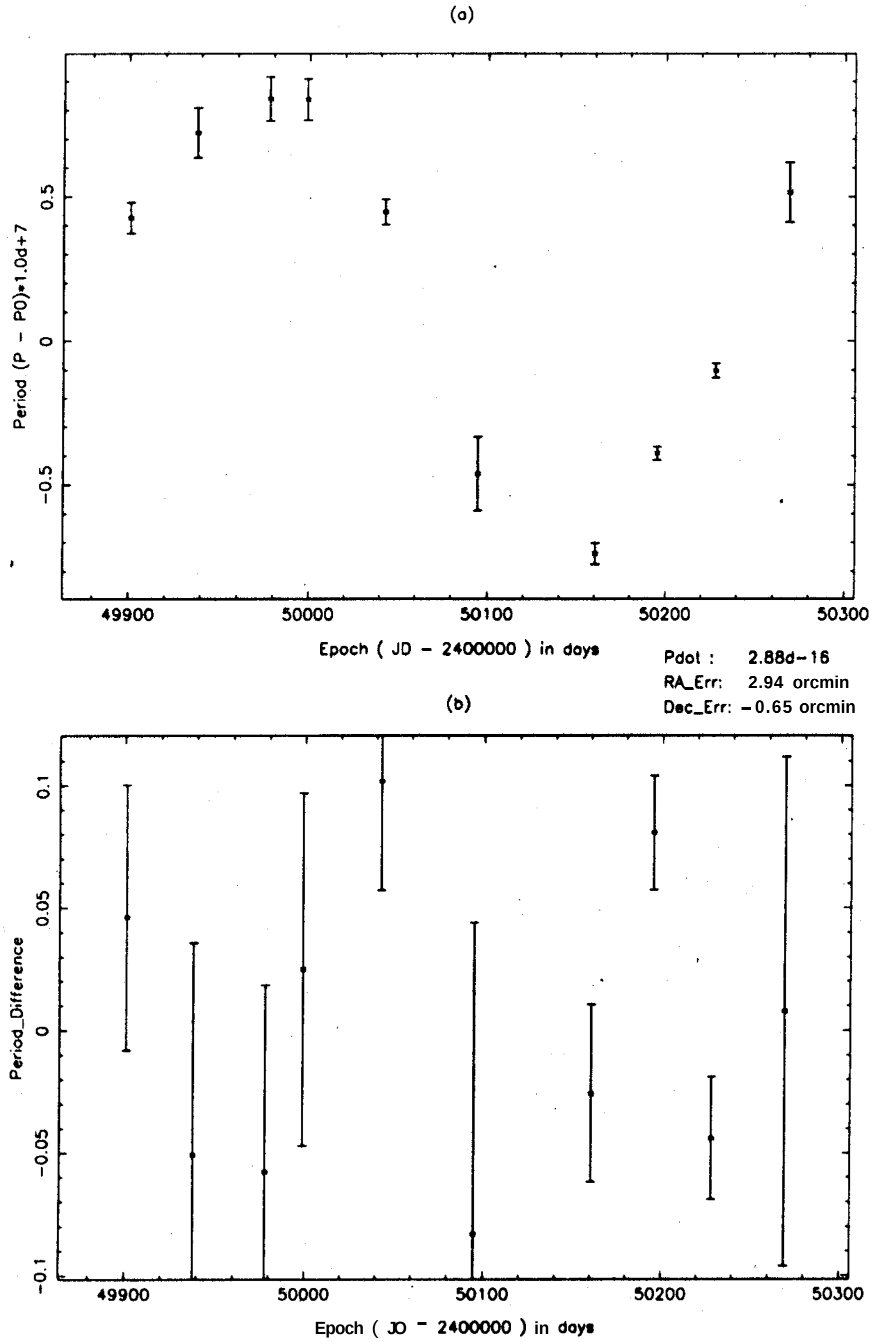

Figure 4.4: Period residuals for PSR J1034-3224. (a) Period vs Epoch plot on which period is estimated over small range of epochs where P0=1.1505904 s. (b) Post-fit period residuals after removing the effect of P and positions errors. The value of the fitted Pdot is given in ss^{-1}.

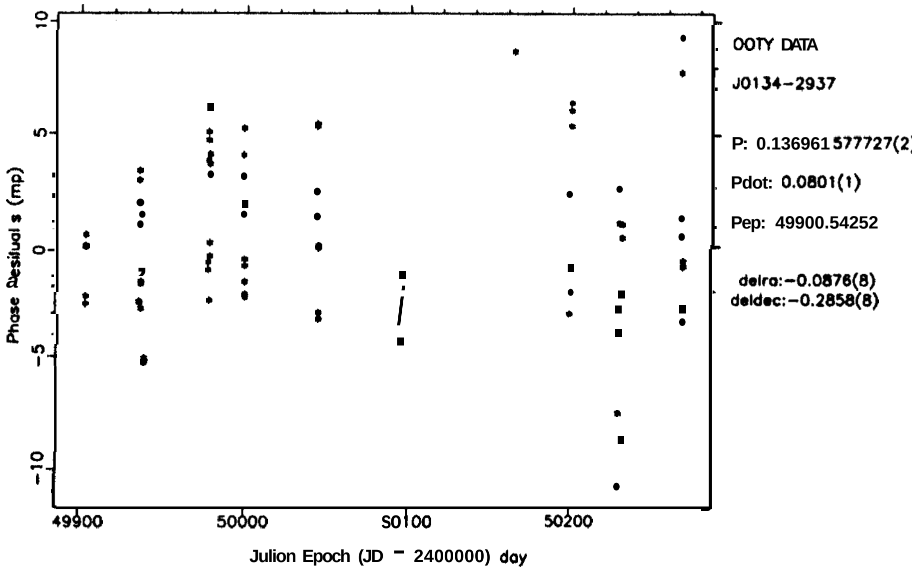

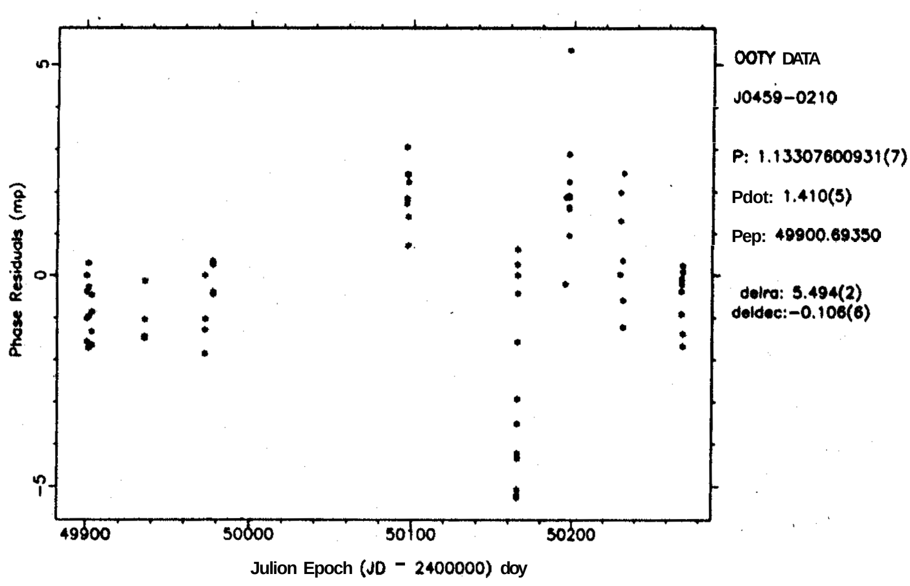

Figure 4.5: **Post-fit** residuals for all the 16 pulsars. The values of the rotation period, P is given in **secs**, $\dot{P}$(**Pdot**) in 10^{-15} ss^{-1}, the reference epoch for the period is in **Truncated** Julian days (JD-2400000) and delra & deldec are the errors in the assumed RA and **Dec** values given in arcminutes. This figure **continues** over the **next** 7 pages.

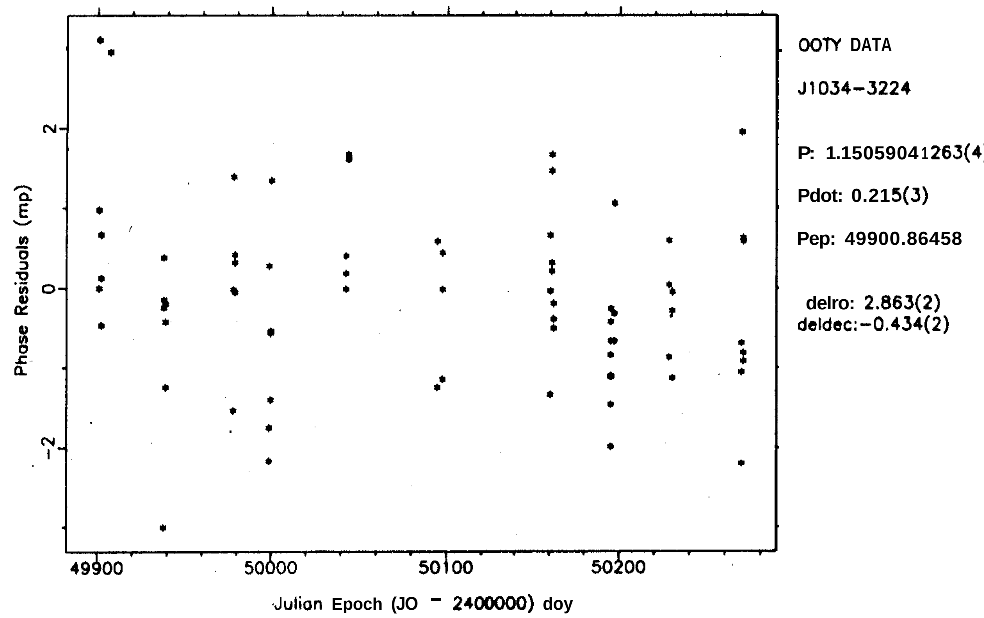
OOTY DATA
J1034-3224
P: 1.15059041263(4)
Pdot: 0.215(3)
Pep: 49900.86458
delro: 2.863(2)
deldec:-0.434(2)
Phase Residuals (mp)
Julian Epoch (JD - 2400000) day
49900
50000
50100
50200
2
0
-2

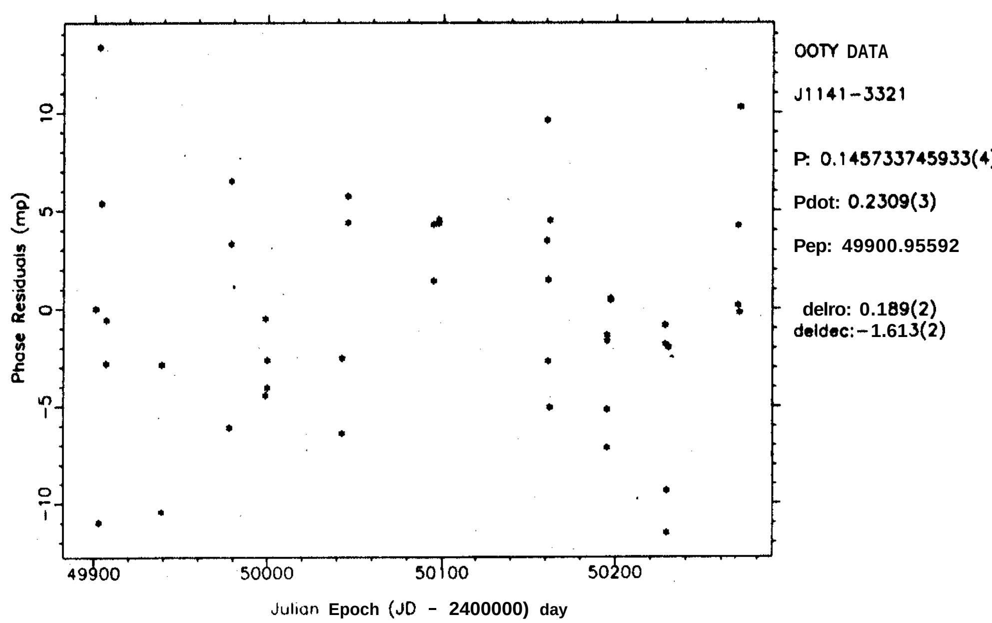
OOTY DATA
J1141-3321
P: 0.145733745933(4)
Pdot: 0.2309(3)
Pep: 49900.95592
delro: 0.189(2)
deldec:-1.613(2)
Phase Residuals (mp)
Julian Epoch (JD - 2400000) day
49900
50000
50100
50200
10
5
0
-5
-10

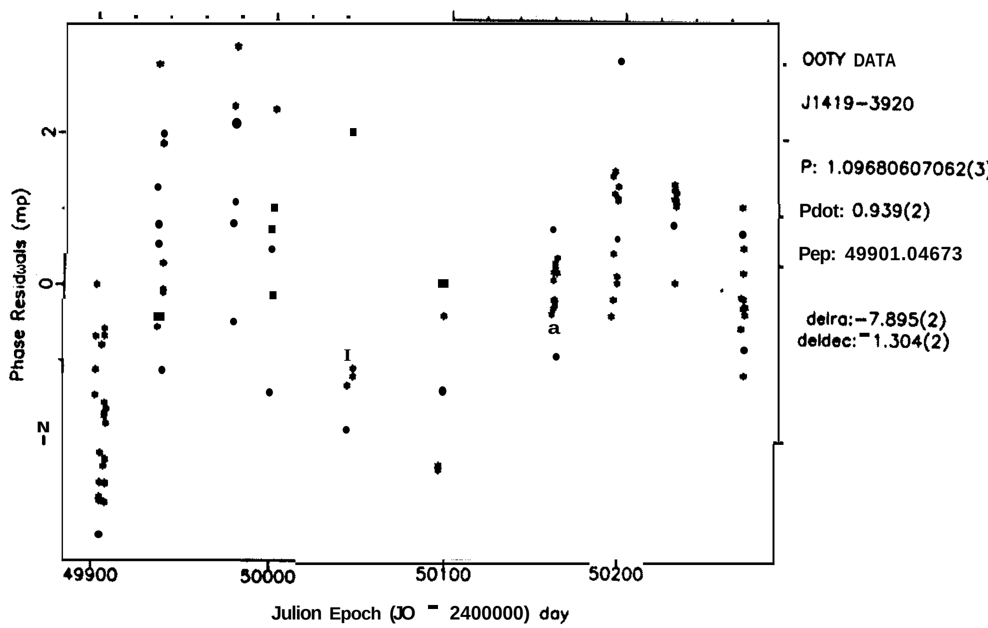
OOTY DATA
J1419−3920
P: 1.09680607062(3)
Pdot: 0.939(2)
Pep: 49901.04673
delra:−7.895(2)
deldec:−1.304(2)
Phase Residuals (mp)
2
0
−2
49900
50000
50100
50200
Julion Epoch (JD − 2400000) day

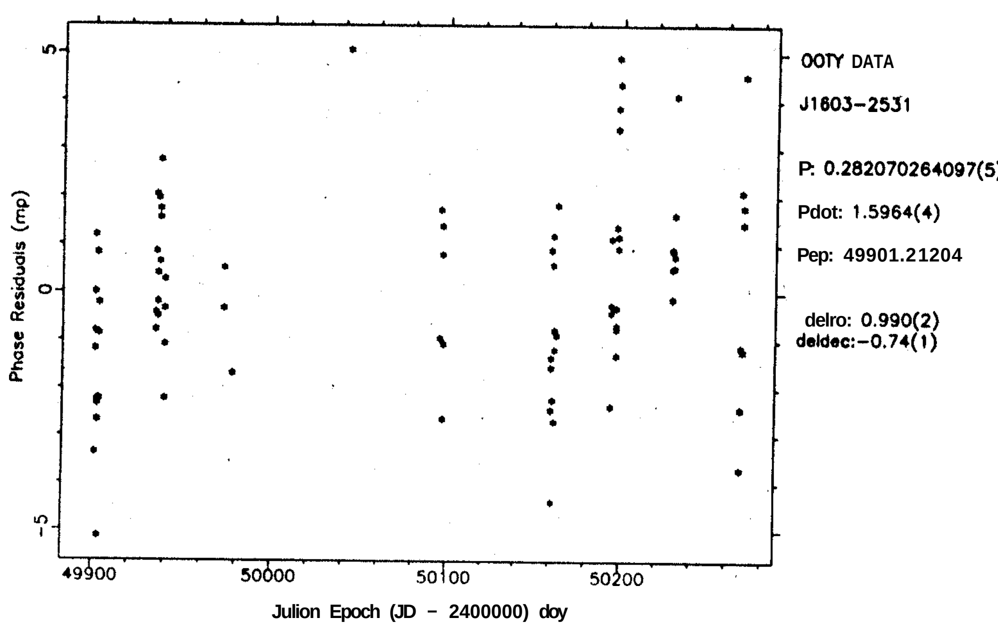
OOTY DATA
J1603−2531
P: 0.282070264097(5)
Pdot: 1.5964(4)
Pep: 49901.21204
delra: 0.990(2)
deldec:−0.74(1)
Phase Residuals (mp)
5
0
−5
49900
50000
50100
50200
Julian Epoch (JD − 2400000) day

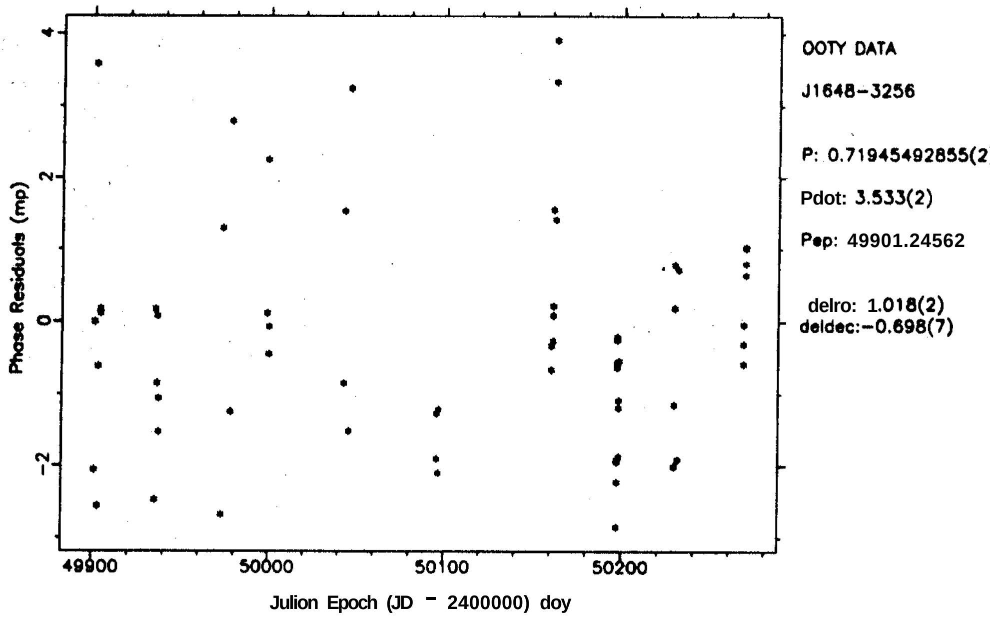
OOTY DATA
J1648-3256
P: 0.71945492855(2)
Pdot: 3.533(2)
Pep: 49901.24562
delro: 1.018(2)
deldec:-0.698(7)
Phase Residuals (mp)
4
2
0
-2
49900
50000
50100
50200
Julian Epoch (JD - 2400000) day

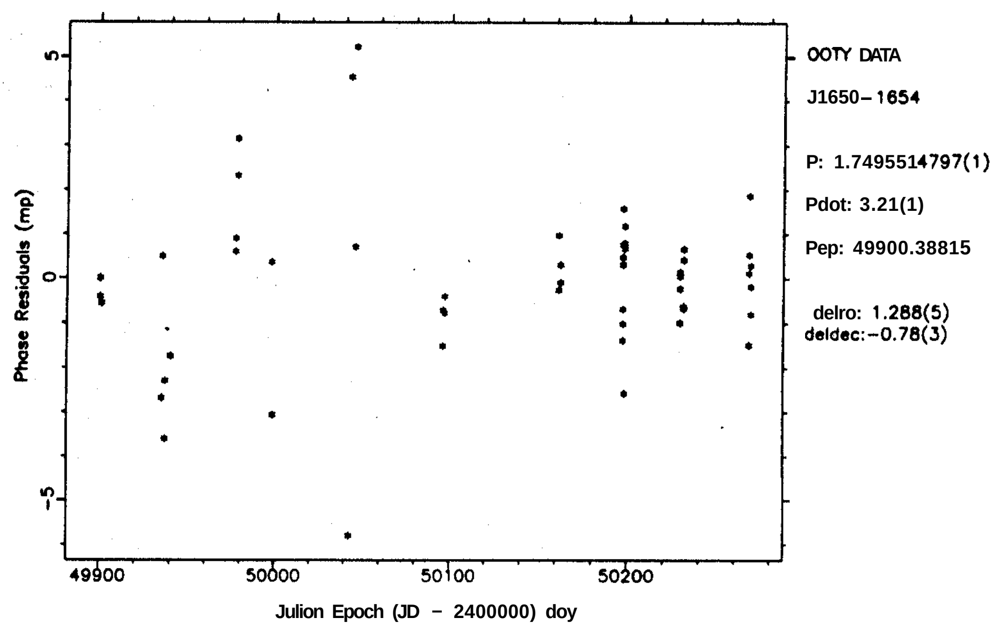
OOTY DATA
J1650-1654
P: 1.7495514797(1)
Pdot: 3.21(1)
Pep: 49900.38815
delro: 1.288(5)
deldec:-0.78(3)
Phase Residuals (mp)
5
0
-5
49900
50000
50100
50200
Julian Epoch (JD - 2400000) day

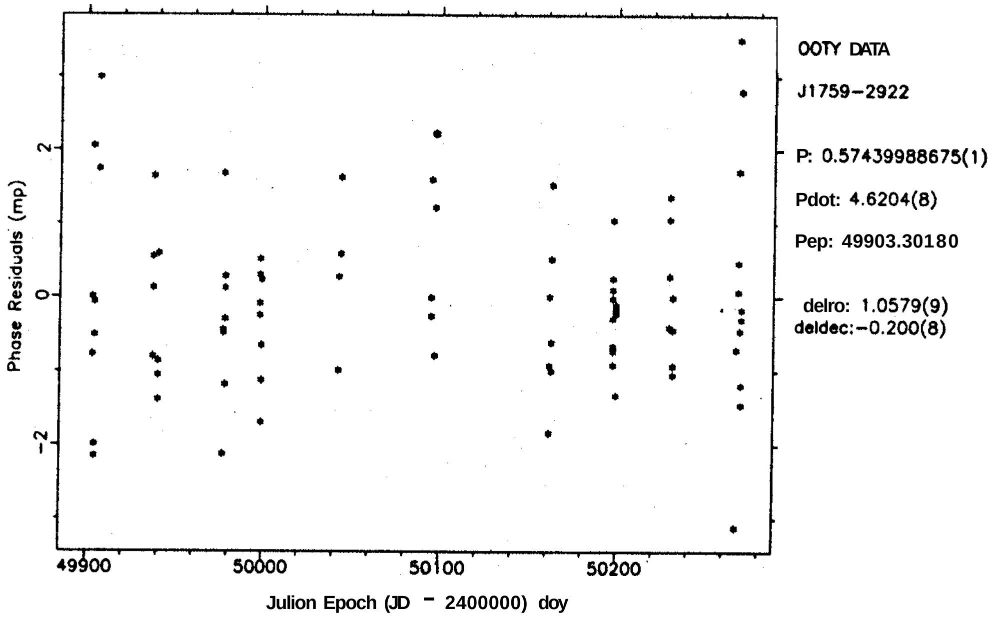
OOTY DATA
J1759-2922
P: 0.57439988675(1)
Pdot: 4.6204(8)
Pep: 49903.30180
delro: 1.0579(9)
deldec:-0.200(8)
Phase Residuals (mp)
2
0
-2
49900
50000
50100
50200
Julion Epoch (JD - 2400000) doy

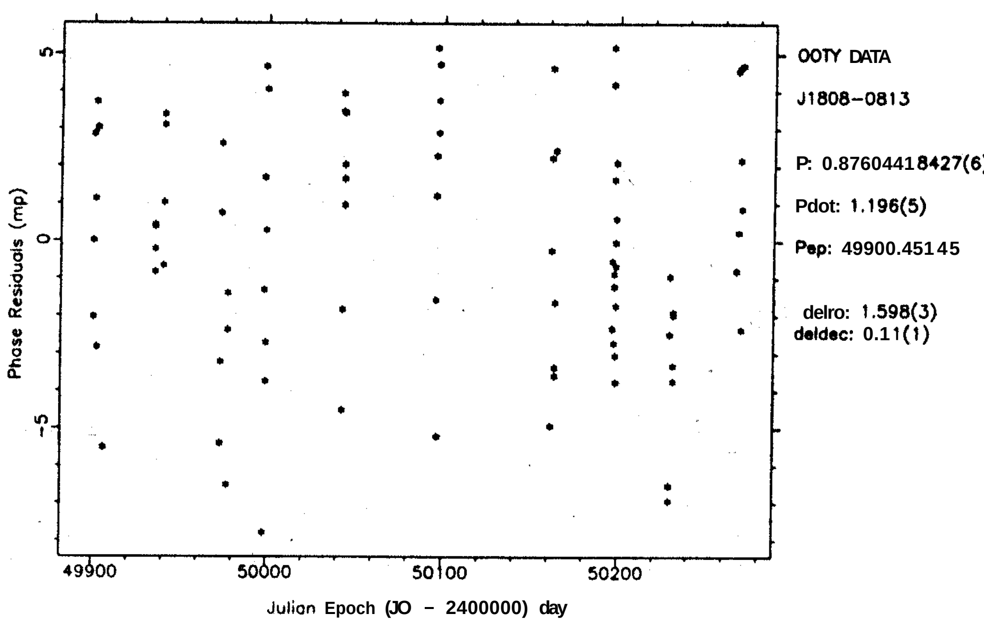
OOTY DATA
J1808-0813
P: 0.87604418427(6)
Pdot: 1.196(5)
Pep: 49900.45145
delro: 1.598(3)
deldec: 0.11(1)
Phase Residuals (mp)
5
0
-5
49900
50000
50100
50200
Julion Epoch (JO - 2400000) day

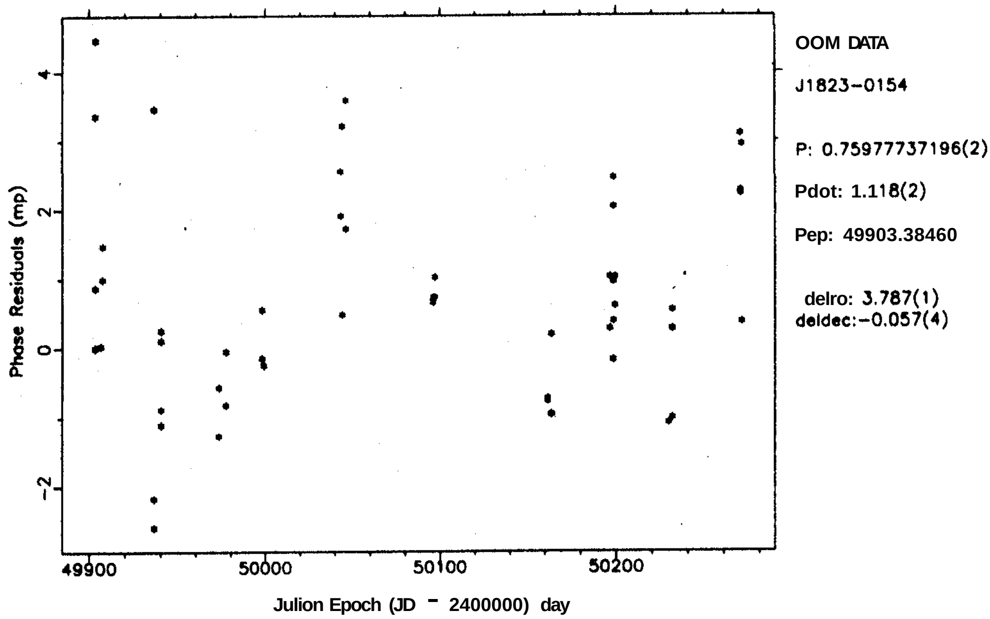
OOM DATA
J1823-0154
P: 0.75977737196(2)
Pdot: 1.118(2)
Pep: 49903.38460
delro: 3.787(1)
deldec:-0.057(4)
Phase Residuals (mp)
4
2
0
-2
49900
50000
50100
50200
Julion Epoch (JD - 2400000) day

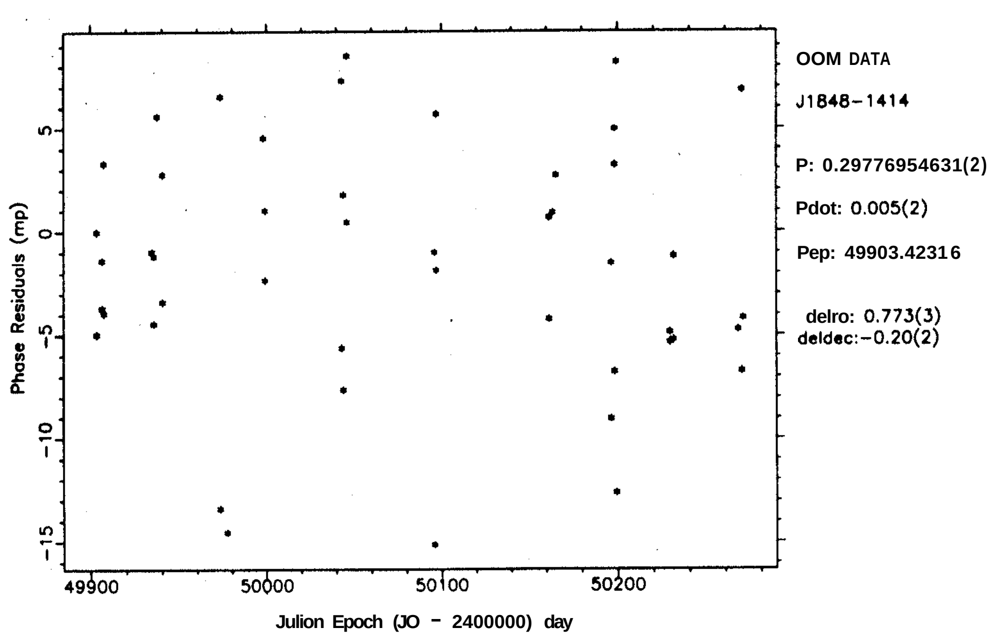
OOM DATA
J1848-1414
P: 0.29776954631(2)
Pdot: 0.005(2)
Pep: 49903.42316
delro: 0.773(3)
deldec:-0.20(2)
Phase Residuals (mp)
5
0
-5
-10
-15
49900
50000
50100
50200
Julion Epoch (JO - 2400000) day

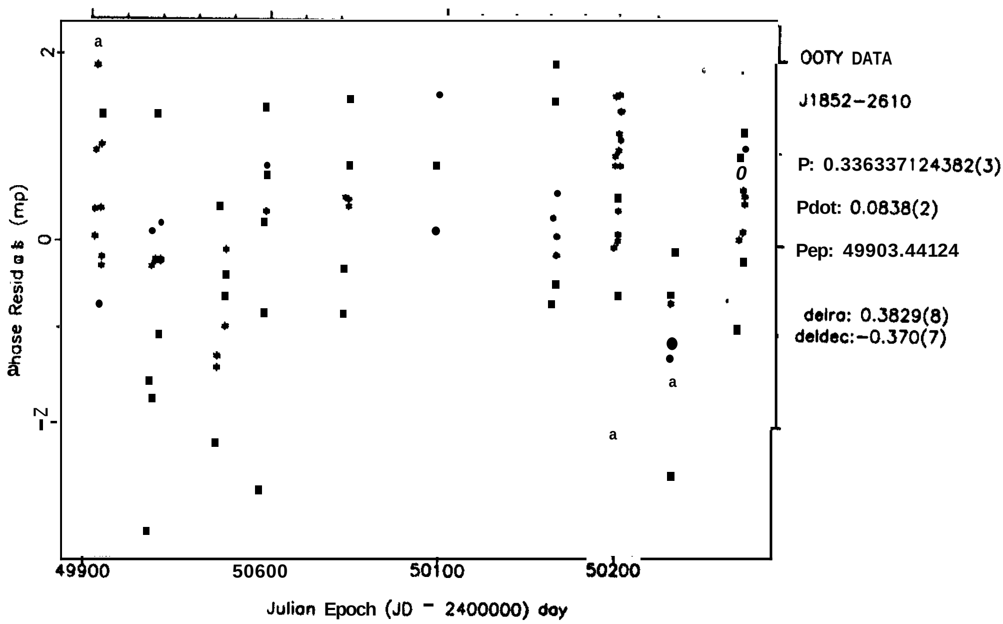

OOTY DATA
J1852-2610
P: 0.336337124382(3)
Pdot: 0.0838(2)
Pep: 49903.44124
delra: 0.3829(8)
deldec:-0.370(7)
Phase Residuals (mp)
Julian Epoch (JD - 2400000) day
49900
50600
50100
50200

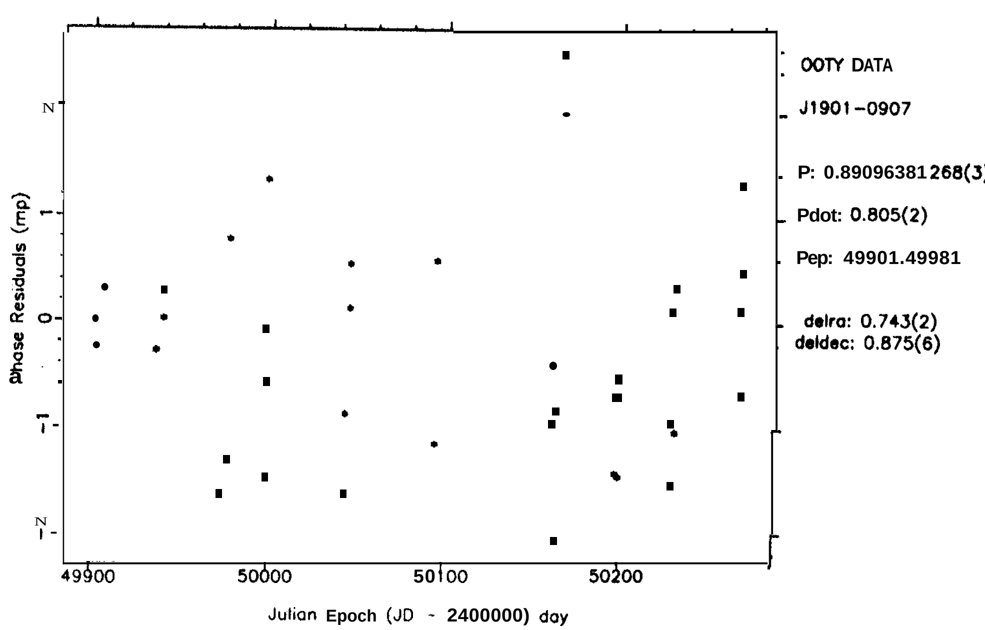

OOTY DATA
J1901-0907
P: 0.89096381268(3)
Pdot: 0.805(2)
Pep: 49901.49981
delra: 0.743(2)
deldec: 0.875(6)
Phase Residuals (mp)
Julian Epoch (JD - 2400000) day
49900
50000
50100
50200

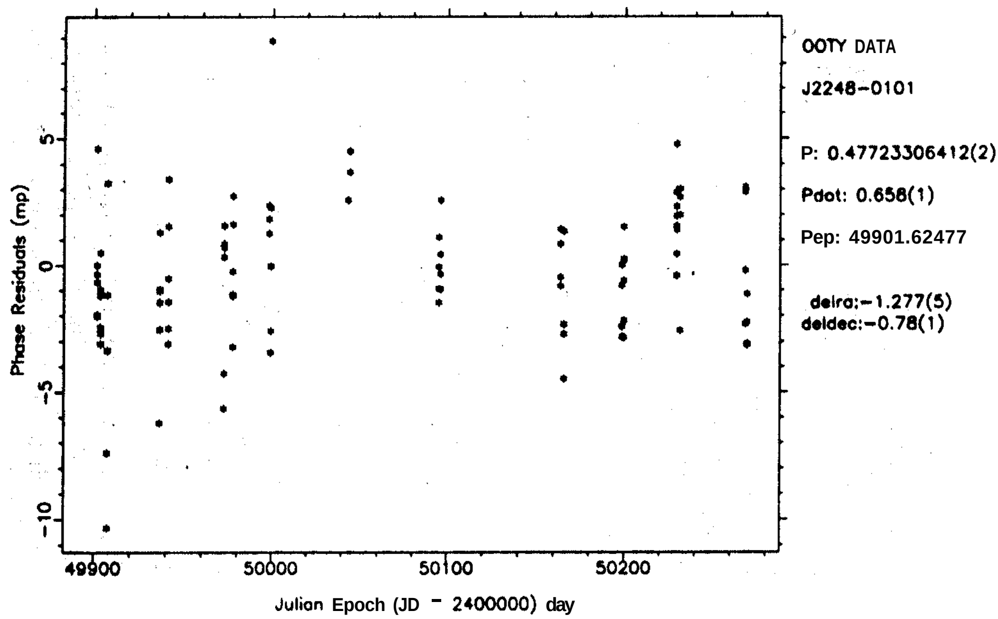
OOTY DATA
J2248−0101
P: 0.47723306412(2)
Pdot: 0.658(1)
Pep: 49901.62477
delra:−1.277(5)
deldec:−0.78(1)
Phase Residuals (mp)
Julian Epoch (JD − 2400000) day

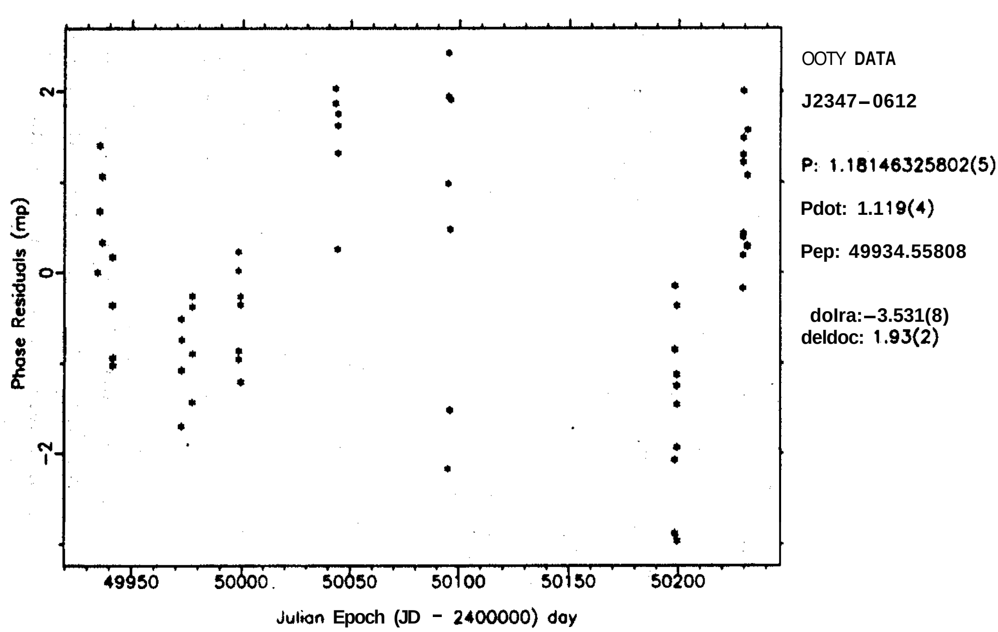
OOTY DATA
J2347−0612
P: 1.18146325802(5)
Pdot: 1.119(4)
Pep: 49934.55808
dolra:−3.531(8)
deldoc: 1.93(2)
Phase Residuals (mp)
Julian Epoch (JD − 2400000) day

Pulsar Name (J2000)	DM (pc cm^{-3})	Period (s)	Period Derivative (10^{-15} ss^{-1})	Reference Epoch (JD)	$\log(\tau_{ch})$ (τ_{ch} in yr)	$\log(B)$ (B in Gauss)
J0134-2937	22(2)	0.136961577727(2)	0.0801(1)	2449900.54252	7.4	11.0
J0459-0210	14(3)	1.13307600931(7)	1.410(5)	2449900.69350	7.1	12.1
J1034-3224	48(3)	1.15059041263(4)	0.215(3)	2449900.86458	7.9	11.7
J1141-3321	46.5(4)	0.145733745933(4)	0.2309(3)	2449900.95592	7.0	11.3
J1419-3920	61(3)	1.09680607062(3)	0.939(2)	2449901.04673	7.3	12.0
J1603-2531	53(1)	0.283070264097(5)	1.5964(4)	2449901.21204	6.5	11.8
J1648-3256	129(2)	0.71945492855(2)	3.533(2)	2449901.24562	6.5	12.2
J1650-1654	46(5)	1.7495514797(1)	3.21(1)	2449900.38815	6.8	12.3
J1759-2922	79(1)	0.57439988675(1)	4.6204(8)	2449903.30180	6.3	12.2
J1808-0813	151(2)	0.87604418427(6)	1.196(5)	2449900.45145	7.1	12.0
J1823-0154	135(2)	0.75977737196(2)	1.118(2)	2449903.38460	7.0	12.0
J1848-1414	134(1)	0.29776954631(2)	0.005(2)	2449903.42316	9.0	10.6
J1852-2610	58(1)	0.336337124382(3)	0.0838(2)	2449903.44124	7.8	11.2
J1901-0907	73(2)	0.89096381268(3)	0.805(2)	2449901.49981	7.2	11.9
J2248-0101	29(1)	0.47723306412(2)	0.658(1)	2449901.62477	7.1	11.8
J2347-0612	20(5)	1.18146325802(5)	1.119(4)	2449934.55808	7.2	12.1

Table 4.1: The measured rotational and derived parameters for 16 pulsars: Column 1 gives the pulsar names according to the J2000 convention, column 2 lists the dispersion measure, column 3&4 gives the rotational parameters P and P obtained from the timing analysis respectively. Column 5 gives the reference epoch for P & P measurements. Columns 6 and 7 list the values of the characteristic age (τ_{ch}) and the magnetic field (B) derived respectively using the rotational parameters. The numbers in the paranthesis indicate 1-σ uncertainties in the last digit quoted.

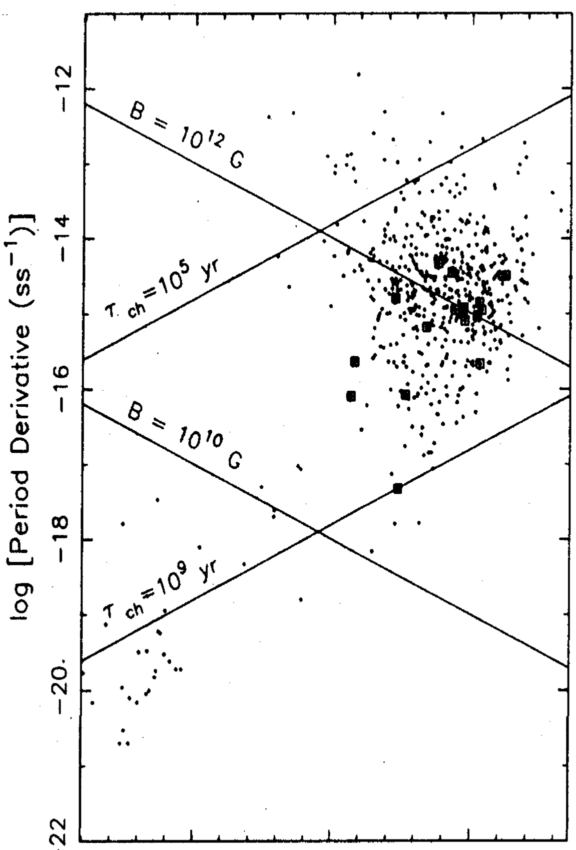

Figure 4.6: Distribution of Pulsars in log($\dot{P}$)-log(P) diagram. The dots enclosed in the squares represent our sample.

the pulsars in our sample are located mostly at large distances from the galactic plane. We expect our sample to help in improving the statistics at such high distances from the galactic plane at the least and possibly in correcting the bias, if any, that may exist against the population at large distances from the galactic plane..

Continued timing observations would be worthwhile in the case of the 4 low-field pulsars (particularly **J1848-1414)**, considering that the region they occupy in the $P - P$ diagram is seen to have significant probability that the pulsar is a member of the binary system. If any of these pulsars is in a binary system, then the orbital period is unlikely to be shorter than one year. If they are in binaries, our estimates of the period derivative and the position offsets would be in error.

4.1.3 Improved Positions

Positions more accurate than were available earlier have been obtained. Fitted offsets to the existing Catalogue positions and the new positions with their errors are given in Table(4.2).

It is important to mention that the telescope we used for our observations responds to only the North-South polarisation component of the signal. Pulsar signal being highly linearly polarised, this limitation results in variations in the observed pulse shapes depending on the ionospheric contributions to the line-of-sight rotation measure during individual observations. However, if the rotation measure to the pulsar is high, we expect such changes to be small considering that there would be sufficient Faraday rotation of the incident polarisation vector across the observed 8 MHz bandwidth. As our observations were made at various hour angles (which should vary the **Faraday** rotation contributed by the ionosphere) we do not expect any systematic pattern to result in the pulse arrival times over the one year span of observations.

It should be pointed out that in some cases our estimates of pulsar positions can be in error larger than that indicated, if there is substantial contribution from 'timing noise' (which **we will** discuss in chapter 5). This is because a substantial fraction **of** the contribution due to the timing noise will have variations (left behind after the second-order fit) which will have one cycle across the span of our observations, which happens to be one year in the present case. However, considering the derived characteristic ages for the pulsars, it seems unlikely that any significant contribution from timing noise may exist in the residuals subjected to position fits. This conclusion will be reassessed in chapter 5.

4.2 Scatter Broadening of Pulses

4.2.1 Introduction

The interstellar **medium** contains irregularities of electron density with a wide range of physical scales. This inhomogeneous medium causes an irregular distortion of the propagating waveform, resulting in scattering of the signal. This **results** in the observer receiving

PulsarName (J2000)	**Position Errors as in the Catalogue**		**Fitted Offset to the positions**		**Improved Coordinates (J2000)**	
	RA h m s	**DEC** ° ' "	**RA** h m s	**DEC** ° ' "	**RA** h m s	**DEC** ° ' "
J0134-2937	00 00 07.00	00 01 00.02	-00 00 **00.351(3)**	-00 00 **17.15(5)**	01 34 **18.649(3)**	-29 37 **17.15(5)**
J0459-0210	00 00 19.94	00 03'59.27	00 00 **21.979(9)**	-00 00 **06.3(4)**	04 59 **51.979(9)**	-02 10 **06.4(4)**
J1034-3224	**00:00:05.01**	**00:01:00.02**	00 00 **11.452(8)**	-00 00 **26.0(1)**	10 **34 19.452(8)**	-32 24 **26.0(1)**
51141-3321	**00:00:14.03**	**00:03:00.07**	00 00 **00.759(6)**	-00 01 **36.8(1)**	11 41 **42.759(6)**	-33 22 **36.8(1)**
51419-3920	**00:00:06.99**	00 01 00.02	-00 00 **31.579(7)**	-00 01 **18.3(2)**	14 18 **50.421(7)**	-39 21 **18.3(2)**
51603-2531	00 00 19.94	00 03 00.07	00 00 **03.958(9)**	-00 00 **44.55(6)**	16 03 **04.959(9)**	-25 31 **44.55(6)**
51648-3256	00 00 25.03	00 04 59.08	00 00 **04.073(8)**	-00 00 **41.9(5)**	16 48 **06.073(8)**	-32 56 **41.9(5)**
J1650-1654	00 00 25.03	00 00 59.08	00 00 **05.15(2)**	-00 00 **47(2)**	16 50 **27.15(2)**	-16 54 **47(2)**
J1759-2922	00 00 14.03	00 03 00.07	00 00 **04.231(4)**	-00 00 **12.0(5)**	17 59 **48.231(4)**	-29 22 **12.0(5)**
518080813	00 00 19.94	00 03 59.27	00 00 **06.39(1)**	00 00 **06.3(7)**	18 08 **09.39(1)**	-08 12 **53.7(7)**
J1823-0154	00 00 19.94	00 04 59.08	00 00 **15.146(5)**	-00 00 **03.4(2)**	18 23 **52.146(5)**	-01 **54 03.4(2)**
J1848-1414	00 00 02.03	00 04 59.08	00 00 **03.09(1)**	-00 00 **12(1)**	18 48 **39.09(1)**	-14 14 **12(1)**
J1852-2610	00 00 25.03	00 04 59.08	00 00 **01.531(3)**	-00 00 **22.2(4)**	18 52 **59.531(3)**	-26 10 **22.2(4)**
51901-0907	00 00 12.01	00 03 00.07	00 00 **02.974(6)**	00 00 **52.5(4)**	19 01 **52.974(6)**	-09 06 **07.5(4)**
J2248-0101	00 00 06.00	00 02 00.05	-00 00 **05.11(2)**	-00 00 **46.7(7)**	22 48 **26.89(2)**	-01 01 **46.7(7)**
52347-0612	00 00 14.99	00 03 00.07	-00 00 **14.13(3)**	00 01 **56(1)**	23 46 **50.88(3)**	-06 10 **04(1)**

Table 4.2: Improved positions for the 16 **Pulsars:** Column 1 **lists** the **J2000** names, columns 2 and 3 list the errors in the pulsar positions as quoted in the Catalogue, and columns 4 and 5 list the best-fit RA and Dec **offsets** computed from our timing data. Columns 6 and 7 give the refined positions. **1-σ** errors indicated in paranthesis are the uncertainties in the last quoted digit.

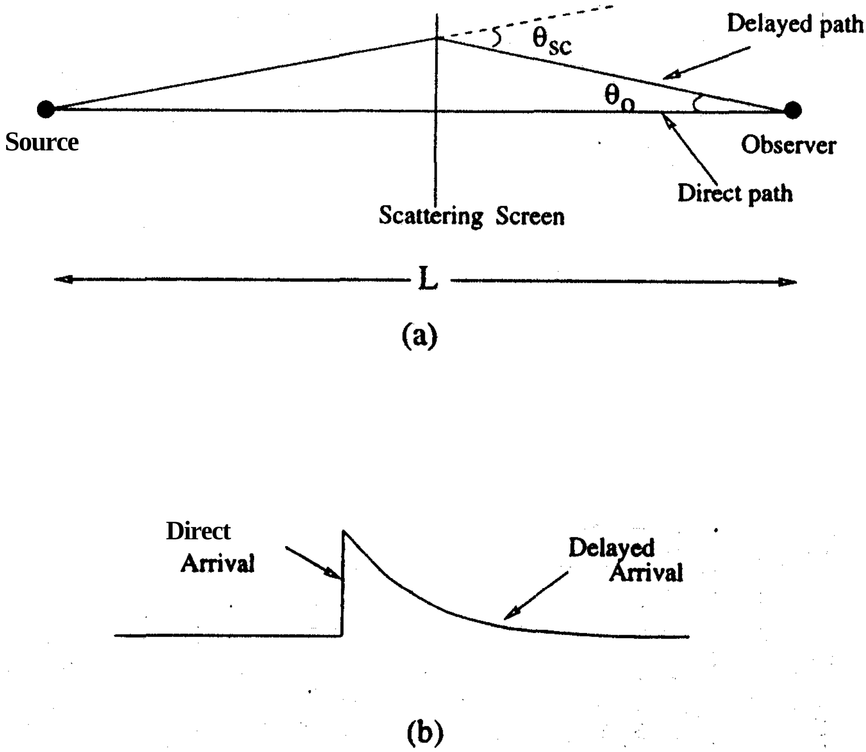

Figure 4.7: (a) Schematic diagram for the scattering mechanism (b) Scattered pulse profile (for zero intrinsic width)

---

the signal for a longer time than the pulse width at emission, due to multipath propagation caused by scattering. As a result the observed pulse gets broadened. Also, at a given time of observation the received signal corresponds not just to a **single** instant of emission but to a range of emission times of duration $\sim \tau_{sc}$, the scattering width. This corresponds to a range of phases in the received signal, of width $\sim 2\pi\nu\tau_{scat}$, where ν is the **observing** frequency. Interference of signals with this phase range produces **patches** of enhanced and reduced intensity. Relative to this intensity pattern a **motion** of the observer due to the Earth's motion, the motion of the pulsar or of the medium itself, will result in variations of the observed intensity. This effect is known as Diffractive Interstellar Scintillation. It was **Scheuer(1968)** who first pointed out that such intensity variations are seen for pulsars on time scales of few minutes to hours, depending upon the observed radio frequency. Thus by studying the different manifestations of the interstellar scattering, such as temporal broadening of pulses, **angular** broadening of the source and scintillation **(Rickett** 1977, **1990)**, one can hope to study the density fluctuations in the interstellar medium **(see** for example, **Alurkar, Slee** & Bobra 1986, Gwinn, Bartel & Cordes 1993).

The process of scattering is illustrated in **fig(4.7a)**. For simplicity, one can assume that the scattering medium is a thin screen containing electron density irregularities of a scale size *'a'* and that it lies half-way along the line of sight between the observer and the source. One can then derive the width of the scattered signal τ_{sc} to be (see Manchester & Taylor 1977)

$$\tau_{sc} = \frac{L\theta^2}{c} \approx \frac{1}{ac}\left(\frac{e^2\Delta n_e}{4\pi m_e}\right)^2 \frac{L^2}{\nu^4} \tag{4.5}$$

where a is the size of the irregularity, An, is the density fluctuation, m_e is the mass of the electron and ν is the observing frequency. The signal arriving by the direct route arrives first, creating the sharp rise while the signals arriving by delayed routes and with diminishing intensity create the exponential tail (fig 4.7b). Scattered pulse profiles of this type are readily observed particularly at longer wavelengths because of the ν^{-4} dependence.

The true distribution of irregularities in the interstellar medium is, however, not one with a single characteristic scale, but is closer to a power law. In wavenumber space, the irregularity spectrum is usually written as

$$P(q) = c_n^2 q^{-\beta} \qquad \text{where} \quad q = \frac{2\pi}{a} \tag{4.6}$$

For a pure Kolmogrov spectrum arising out of turbulence, $\beta = \frac{11}{3}$, which yields $\tau_{sc} \propto \nu^{-4.4}$ (see Sutton 1971).

4.2.2 Measurement Procedure

The average profile was obtained for each pulsar as explained in chapter 3 and the scatter broadening was estimated using a least-square fit to the observed average profile with the following well known model. The observed pulse profile $y(t)$ is the convolution of intrinsic pulse shape $x(t)$ with: (a) the impulse response, $S(t)$, characterising the scatter broadening in the ISM; (b) the function, $d(t)$, describing the dispersion smearing across the narrow spectral channel; and (c) the instrumental impulse response $i(t)$. That is,

$$y(t) = x(t) \otimes s(t) \otimes d(t) \otimes i(t) \tag{4.7}$$

where $\otimes$ denotes convolution operation. If one assumes that the scattering material is concentrated in a region whose thickness is very small compared to the distance to the pulsar and the observer (thin screen approximation), then the impulse response characterising the interstellar scatter broadening can be written as

$$s(t) = \exp(-t/\tau_{sc}) \tag{4.8}$$

For the purpose of modelling, the intrinsic pulse shape is assumed to be a gaussian with half-power width w_o. The template of the scatter broadened pulse profile can be produced by convolving the different responses with a gaussian as given by equation(4.7). The dispersion smearing (due to the finite width of the frequency channels) is considered corresponding to the channel width of 32 KHz. Many different combinations of τ_{sc} and w_o were tried in a suitable grid search to look for the best match between the observed average pulse and the predicted pulse template. In some cases, where it was suspected that the intrinsic pulse profile may have two components, we assumed an intrinsic pulse profile consisting of two gaussians with an assumed separation while solving for the ratio of their heights and a common value for their widths. Even in other cases, a model with two pulse components was assessed on the basis of the goodness of fit. The best fit was produced by minimizing the normalised χ^2 value defined by,

$$\chi^2 = \frac{1}{N_{\mathrm{dof}}\sigma_{\mathrm{n}}^2} \sum_{i=1}^{N} [y_i^{\mathrm{o}}(t) - y_i^{\mathrm{m}}(t)]^2 \tag{4.9}$$

where, a, is the root mean square noise value of the offpulse, y^{o} is the observed pulse profile and y^{m} is the model pulse profile. The y^{m} profile is similar to $y(t)$ except an amplitude scale factor and a constant offset in phase and baseline that minimizes χ^2. N is the number of points used, and N_{dof} is the number of degrees of freedom.

4.2.3 Results and Discussion

Out of the 708 pulsars listed in the Pulsar Catalogue by Taylor et al. (1993; updated version, 1995) measurement of temporal broadening exists for only 148 pulsars. Recently, Ramachandran et al.(1997) have measured scattering widths for 26 more pulsars at 327 MHz. Using our present observation, we have obtained estimates of the scatter broadening for 10 pulsars. A few of these were also studied by Ramachandran et al. and our estimates are found to be consistent with the earlier measurements.

Figures (4.8 and 4.9) show the observed pulse profiles at 327 MHz superimposed by a dotted curve indicating the best-fit profile based on the model described above. The results of the analysis are listed in Table (4.3).

One of the conventional methods of examining the scattering properties along various lines of sight is to plot the dispersion measure versus the measured scatter broadening. Figure (4.10) shows such a plot showing τ_{sc} (at 400 MHz) versus DM for 172 pulsars, including our 10 measurements. The open circles indicate the scatter broadening estimates based on the decorrelation bandwidth measurements, crossed circles represent our scatter broadening measurements with the ORT and filled circles indicate earlier direct measurements of scatter broadening. The *r,* values are scaled to 400 MHz assuming a frequency dependence of $\nu^{-4.4}$.

A line-fit for the direct τ_{sc} measurements (filled circles) show a slope of 4.3±0.4, and the corresponding slope for τ_{sc} estimated through the decorrelation bandwidth measurements is 2.7±0.3 (Ramachandran et al. 1997). The decorrelation bandwidth measurements available for pulsars with DM > 100 pc cm^{-3} seem to suggest that the steepening of the τ_{sc} with DM is real and is not related to the coincidence that the dependence appears to change with the kind of measurement used. Sutton (1971) and Rickett (1977) have noted that for DM $\leq$ 20 pc cm^{-3} the measured scattering delay increases roughly as DM^2, but for 20 $\leq$ DM $\leq$ 400 pc cm^{-3} the relationship steepens considerably, to give a slope of about 4. This is the signature seen in figure(4.10), but the slope change occurs around $\sim$ 100 pc cm^{-3}.

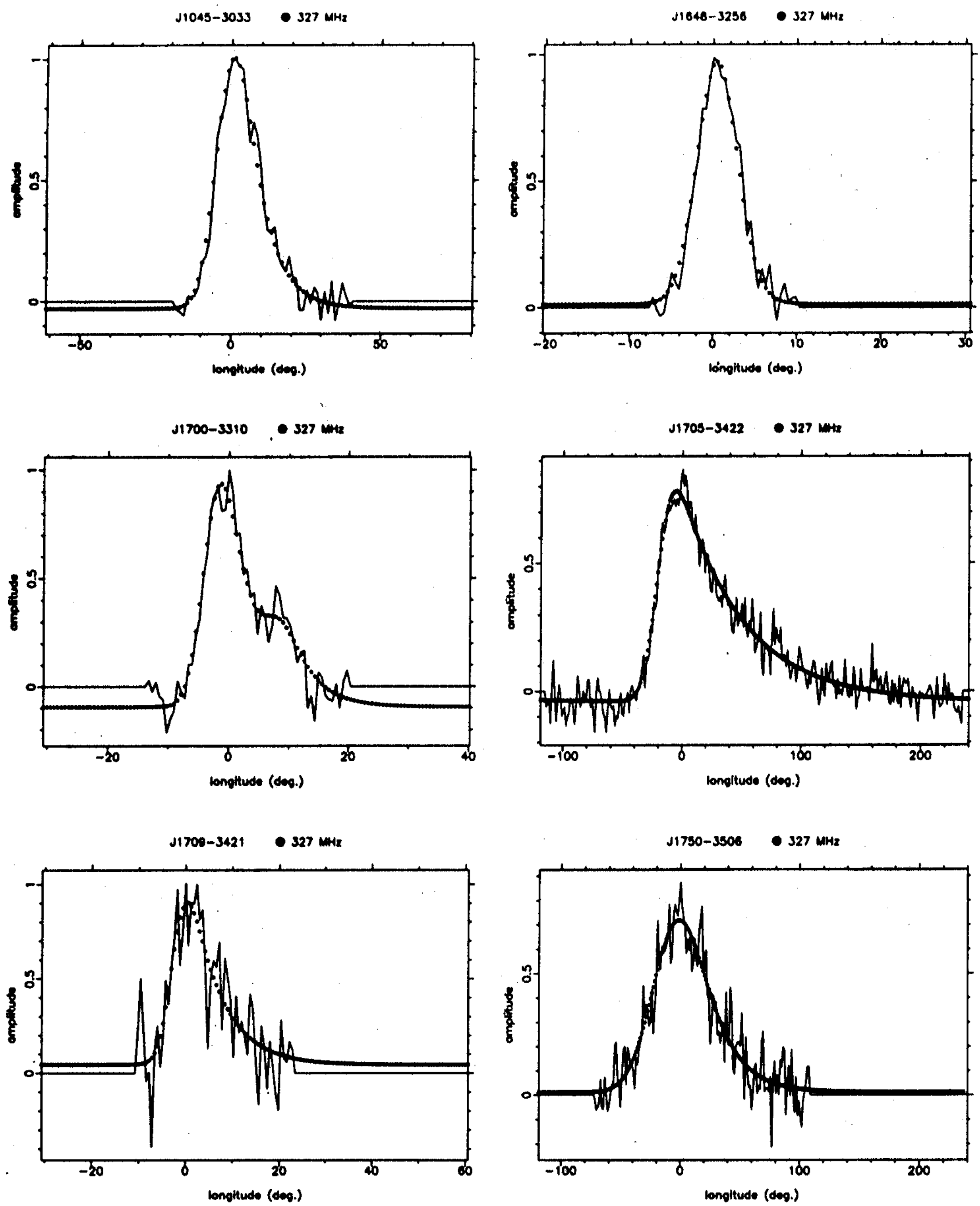

Figure 4.8: The observed pulse profiles at 327 MHz and the dotted line shows the best-fit model for the pulse.

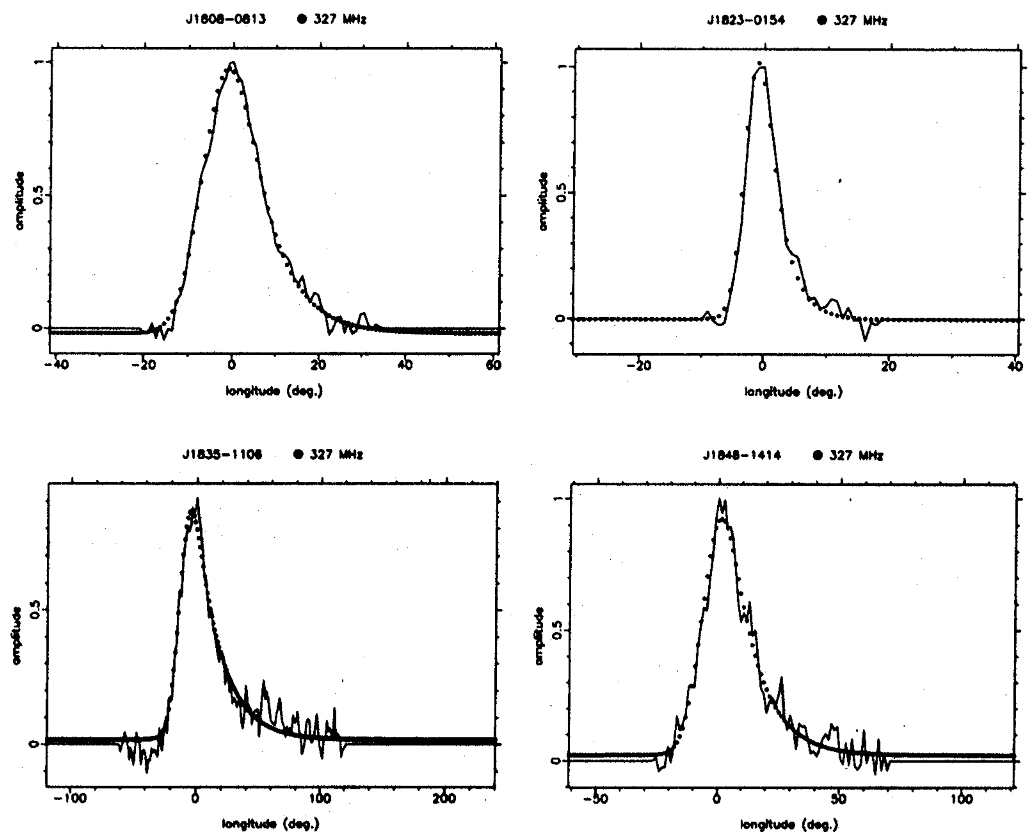

Figure 4.9: Continuation of the scattered pulse profiles

Pulsarname (J2000)	Period (s)	DM (pc cm^{-3})	Intrinsic Width		Scattering Delay		$\Delta(w_o + \tau_{sc})$ (ms)	Width as given in the Catalogue	τ_{exp} (ms)	χ^2
			w_o (ms)	Δw_o (ms)	τ_{sc} (ms)	$\Delta\tau_{sc}$ (ms)				
J1045-3033	0.33033	52.9	11.6	2.8	6.6	2.7	1.5	16.0	0.04	1.04
J1648-3256	0.71946	129.0	12.0	1.5	1.8	$\tau_{sc} < 5.8$	1.1	17.0	6.7	1.52
J1700-3310*	1.3583	171.0	22.4	15.9	9.2	$\tau_{sc} < 25.5$	4.8	56.0	17.6	1.4
J1705-3422	0.25542	145.0	18.1	3.2	38.2	4.8	2.9	21.0	10.7	1.47
J1709-3421	0.6921	188.0	12.0	12.8	12.6	$\tau_{sc} < 27.5$	9.6	56.0	25.5	1.44
J1750-3506	0.68401	195.0	93.3	28.0	41.0	$\tau_{sc} < 67.0$	18.3	76.0	31.3	1.22
J1808-0813	0.87604	151.0	30.8	31.5	17.7	2.2	1.8	29.0	9.4	1.04
J1823-0154	0.75978	135.0	9.8	2.0	5.7	1.4	1.2	15.0	8.5	2.6
J1835-1106	0.16591	132.0	7.8	1.2	9.4	1.5	0.8	7.2	13.1	2.2
J1848-1414	0.29777	134.0	13.5	2.6	9.4	2.8	1.9	14.0	7.8	1.47

Table 4.3: The table lists against the name of each pulsar its rotation period, dispersion measure, an estimate of the intrinsic width (w_o) and its error bar and the estimated scatter broadening (τ_{sc}) and its error, the correlated error on ($\tau_{sc} + w_o$), the width at 436 MHz as given in the catalogue, the expected scatter broadening to the free electron density distribution model of Taylor & Cordes (1993) and the value of the minumum χ^2 obtained. The error bars correspond to 99.99% confidence level. The pulsar J1700-3310 has two gaussian components separated by 28 mP and the second component has a relative strength of 0.3 of the main component.

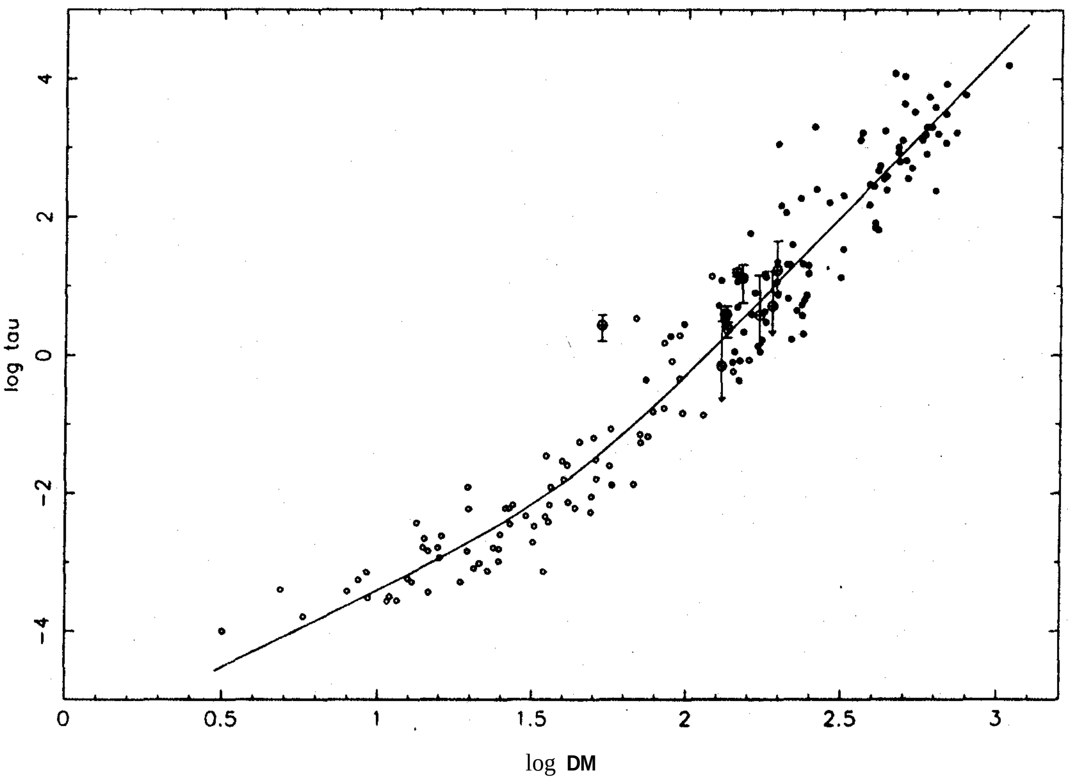

Figure 4.10: Observed scatter broadening as a function of dispersion measure, for 172 pulsars. Plus sign enclosed by circles represent our scattering delay measurements. Open circles represent the scattering delay calculated from the decorrelation band-width measurement with the relation $2\pi\nu\tau_{sc} = 1$, filled circles represent the directly measured scatter broadening. The values corresponding to the open and filled circles are taken from the Princeton pulsar catalogue of Taylor et al.(1995) and from Ramachandran et al.(1997). All the scattering values are scaled to 400 MHz.

The pulsar J1045-3033 shows excessive scatter broadening ($\sim$ 6.6 ms) than what would be expected based on its dispersion measure of 52.9 pc cm^{-3}. This DM corresponds to a distance of $\sim$ 4 kpc according to the Taylor-Cordon electron density model, and gives a z-distance equal to the limiting z-distance beyond which one runs out of the n_e column density. The excess scattering strongly suggests a dominant scatterer along the sight-line. We have tried to see whether such a dominant scatterer could be an extension of the Gum Nebula. In the above model, fluctuation parameter for the electron density in the Gum region is not incorporated. To get an estimate of the fluctuation parameter (F_g) in this region, we have examined the value of the scattering width for the Vela pulsar, which is believed to be behind the Gum Nebula and its distance is known independent of its dispersion measure. We find that F_g of $\sim$ 10 in the Gum region would be appropriate to explain the observed scattering width for the Vela pulsar. If we incorporate this value of the fluctuation parameter ($\sim$ 10) and consider an increase in the extent of the Gum region from a radius of $\sim$ 21° (as in the Taylor-Cordes model) to $\sim$ 28° to allow the pulsar sight-line to cross the 'extended' Gum region, we find that the observed scattering width can be explained well. This would also then imply that the pulsar is actually much closer (at 0.54 kpc) rather than at 4.17 kpc.

Allowing for a possibility that this excess scattering is not due to the Gum Nebula, we look for the possibility of an ionised hydrogen region (HII region) produced by some star close to the line of sight to the pulsar. From the optical imago of the region close to the pulsar, the closest star (spectral type KO) found is at a separation of 7' from the pulsar sight-line. If we want to associate the excess scattering to this star, then this star should contribute an excess DM of 15–20 pc cm^{-3} if its assumed to lie half the distance to the pulsar. Normally HII regions are more prominent in the case of very hot stars such as 'O' type, but Prentice & ter Harr (1969) have extended their calculations of HII regions from 'O' type to 'K3' spectral type stars and the electron density could be of the order of 2 cm^{-3}. We consider it quite unlikely that this star would have an HII region of considerable size for the pulsar sight-line to cross through this region to give the observed excess scattering, although such a possibility cannot be ruled out. Therefore, we would like to associate the scattering region tentatively with the 'extended' Gum region.

4.3 Pulsar Current Analysis

Some statistical studies on pulsars, attempting to derive their birth rate and number distribution as a function of period, magnetic field etc. have been carried out over the past ten years or so. The evolution of pulsars as a function of period and its time derivative was discussed by Phinney & Blandford(1981) and Vivekanand & Narayan(1981) and the latter arrived at a conclusion that some significant fraction of pulsars may be born rotating slowly which they named as ***injected*** pulsars. Deshpande et al.(1995, hereafter D95) have argued that such injected population is evident in the magnetic field range $12 < \log(B) < 12.6$ arid they suggest that these may be recycled pulsars which are released into the pulsar population. Since this analysis by D95, the number of pulsars which can be included in

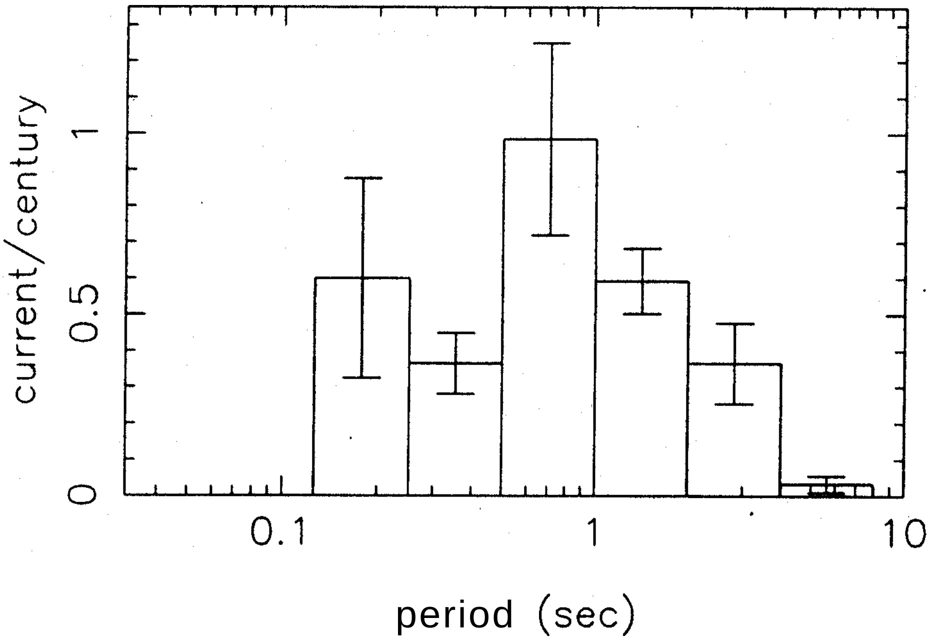

Figure 4.11: The current distribution as a function of period. As may be seen, the current reaches its maximum value around a period of 0.6s. The maximum value of the current corresponds to a pulsar birth rate of about 1 in 100 years.

---

such analysis has increased from from 322 to 443 and therefore it may be worthwhile to assess the result of this improvement in the statistics. With this in mind, we have revisited their analysis including our 16 pulsars in the list and the implications of the recent Parkes Survey.

The birth rate of pulsars can be obtained by looking at the pulsar current over a period bin of width AP, reaching a maximum value, ie., the initial periods of all pulsars rue less than the period under consideration and death of pulsars has not yet set in, then this maximum value of the current represents the *birthrate* of the pulsars (Vivekanand & Narayan 1981). The pulsar current. in a period bin of width A P around a period (P)can be defined as (Phinney & Blandford 1981, Vivekanand & Narayan 1981)

$$J(P) = \sum_{i=1}^{n_{psr}} \frac{S_i \dot{P}_i}{f \Delta P} \tag{4.10}$$

where n_{psr} is the number of known pulsars in the bin, f is the beaming fraction (assumed to be 0.2), $\dot{P}_i$ is the time derivative of the period and S_i is the scale factor (which corrects for the observational selection effects) for the i^{th} pulsar. The procedure to compute the scale factors involves a detailed Monte Carlo simulation (for details refer to Ramachandran 1996, D95).

Fig(4.11) shows the pulsar current as a function of the rotation period P after including the implication of the latest Parkes survey in calculating the scale factor S,. From this

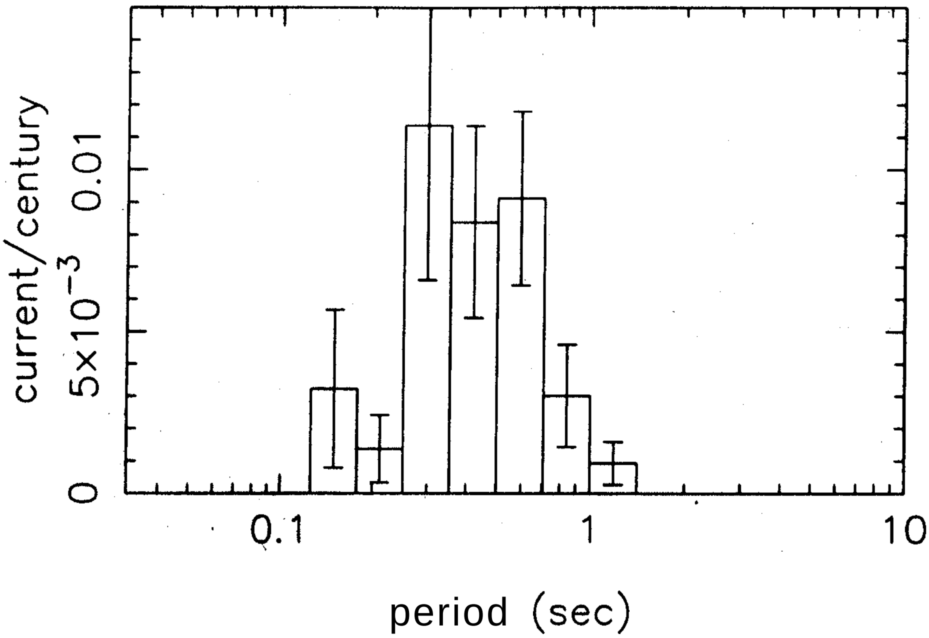

Figure 4.12: The current of pulsars in the field range **log(B)=10.5–11.5.** The birth rate of these pulsars is rougly 1 in **10000** years.

---

figure, noting the maximum current value, we arrive at an estimate of the pulsar birth rate to be one in 100 ± 25 years, which roughly agrees with the earlier values such **as** 75 ± 15 years obtained by D95, 100 years derived by Narayan & Ostriker (1990). Fig(4.12) shows the pulsar current **as** a function of P, for those pulsars whose magnetic fields lie in the range of $10.5 < \log B($ in Gauss$) < 11.5$. Birth rate of pulsars in this magnetic field range appears to be roughly one in 10,000 **years.**

Fig(4.13) shows the distribution of true number of pulsars in the $P - B$ plane. The true number of pulsars in any given bin of width A P around a period P and A B around field B is given by

$$N_B(P) = \frac{1}{f}\sum_{i=1}^{n_{psr}} S(P,\dot{P}_i,z_i) \qquad (4.11)$$

where f is the beaming factor and $S(P,\dot{P}_i,z_i)$ is the scale factor corresponding to the period P, period derivative P and the height z from the plane of the i^{th} pulsar. In the **fig(4.13),** it looks as if the low field pulsars form a distinct island in the true number distribution and there is a valley between the two population of pulsars as already noted in D95. The true number distribution has not changed much after adding 122 more pulsars to the earlier list out of which the number of pulsars added to the distinct island is 13 while the earlier number in this region was 35. This indicates the earlier conclusion of D95 were not a result of a statistical artifact, and that there is most likely a distinct class of pulsars.

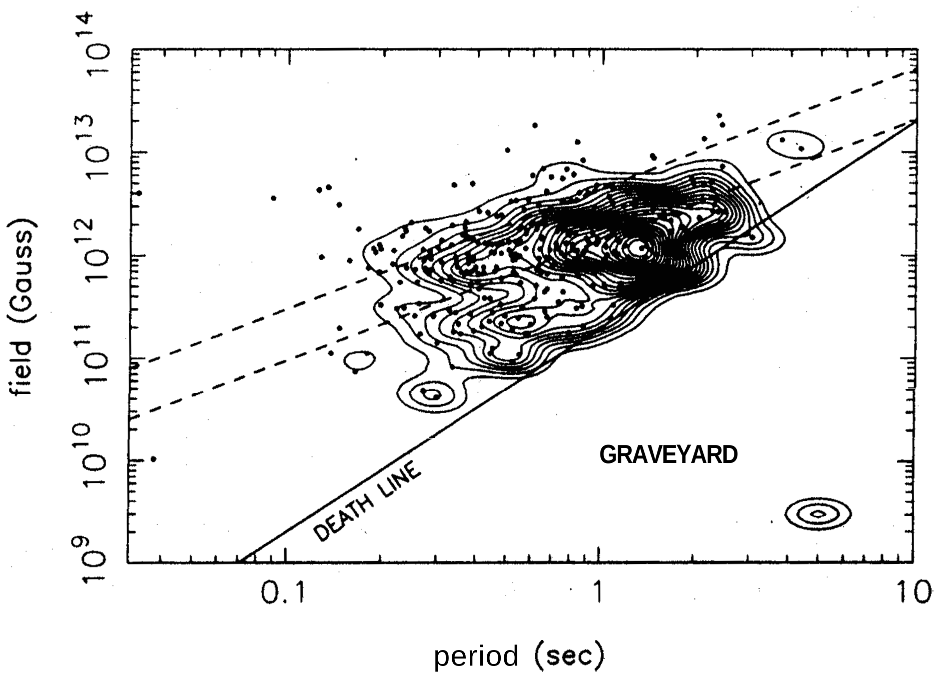

Figure 4.13: The true number distribution as defined by equation(4.11). The contours have been smoothed with a function shown in the bottom right hand corner of the panel. It may be seen that pulsars in the field range log B = 10.5–11.5 appear to form a distinct island; there appears to be a valley between the distribution of these pulsars and the high field pulsars. The two 'dashed' lines are equilibrium period lines; the lower one corresponds to accretion at the Eddington rate, and the upper one to accretion at 10 times the Eddington rate. The dots represent the position of the pulsars.

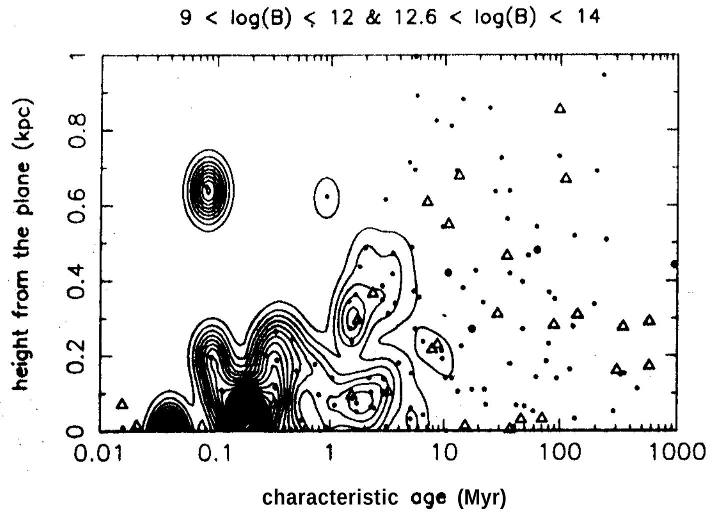

Figure **4.14:** The current of pulsars plotted for all pulsars excluding the magnetic field range $\log(B) = 12.0 - 12.6$. This distribution is easily understandable in terms of the majority of pulsars being born close to the galactic plane and migrating away from it due to velocities acquired at birth. The small filled circles are the pulsars which **were** included in the earlier analysis, open triangles are the new additions and the large filled circles are the ones which belongs to our list.

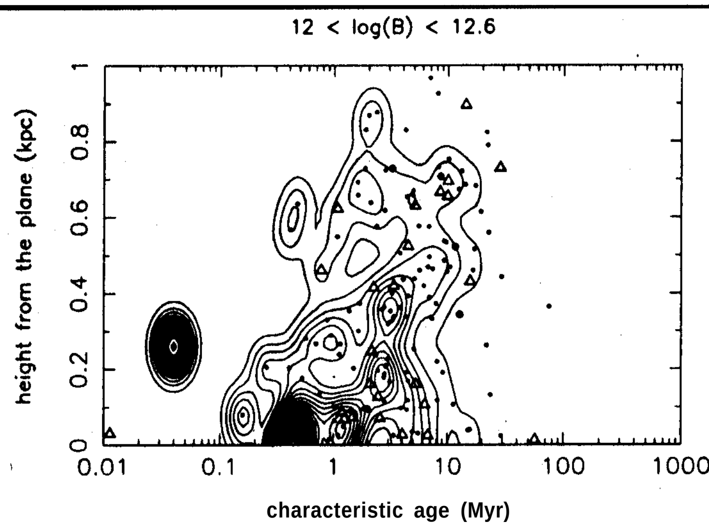

Figure **4.15:** In this figure the current of pulsars in the magnetic field range $12 < \log(B) < 12.6$ alone is shown as a function of characteristic age and height from the plane. This distribution is consistent with the idea of pulsars being **injected** with a characteristic **age** of ~ 1 Myr at a variety of distances from the galactic plane ranging all the way up to 800pc. The open circles are the pulsars which were there in the earlier analysis, open triangles are the new additions from the latest version of the catalogue and the filled circles are our sample of pulsars.

Pulsar current, as a function of characteristic age($\tau_{\rm ch}$) and the distance z from the galactic plane, can be defined as

$$J_z(\tau_{\rm ch}(P,\dot{P})) = \frac{1}{f}\sum_{i=1}^{n_{\rm psr}} \frac{S(P_i,\dot{P}_i,z_i)}{\Delta\tau_{\rm ch}} \tag{4.12}$$

Fig(4.14) shows the current distribution in the $z - \tau_{\rm ch}$ plane for the field range of $9 < \log(B) < 12$ & $12.6 < \log(B) < 14$, which appears consistent with a picture that most of the pulsars being born close to the galactic plane and they migrate from it due to velocities acquired at birth. If one-restricts oneself to pulsars with fields in the range $12 < \log(B) < 12.6$, then the corresponding current distribution (see fig(4.15)) shows that there is an injection of pulsars with a characteristic age of about 1 Myr and injected at large distances (~800 pc) from the galactic plane. The addition of pulsars marked by open triangles and our sample of pulsars marked by filled circles have not changed the result significantly in comparison to the similar analysis carried out by D95. Such a height distribution can be explained if a certain fraction of binaries acquire substantial centre of mass velocities during the first explosion and migrate away from the galactic plane. When they disrupt during second supernova explosion, two pulsars, the first-born one with a characteristic age of a recycled pulsar and the second one with a short characteristic age are released. This would also explain the observation of short characteristic age pulsars moving towards the galactic plane (Harrison et al. 1993).

4.4 PSR B1952+29

We have also studied this pulsar in our timing observations. The observed pulse profile at 327 MHz is plotted in fig(4.16) along with profiles at other available frequencies. This pulsar is one of the classic examples that show significant pulse shape variation with frequency. At low frequencies, only the core component seems to be present and also the pulse width reduces with increasing frequency. At 327 MHz, one of the conal component starts appearing and it gets slightly more prominent at 430 MHz. At still higher frequencies (> 1400 MHz), the core component disappears completely and a clear conal double profile is seen.

PSR B1952+29 falls into a intermediate class of pulsars having a long rotational period as normal pulsars, but with a low period derivative. The rotational period of this pulsar is 0.426676786488(3) secs, and its $\dot{P}$ is 1.64×10^{-18}ss^{-1} at the epoch JD 2448415. One of the puzzling aspect about this pulsar is that the different groups have measured different values of proper motion at different epochs. The proper motion in RA & Dec, i.e. μ_α & μ_δ as, estimated by different workers are 51 ± 51 & 121 ± 64 mas/yr (Mansfield & Rankin 1977), 121 ± 44 & 132 ± 41 mas/yr (Gullahorn & Rankin 1978), 25 ± 17 & -36 ± 10 mas/yr (Lyne et al. 1982). Though the quoted uncertainties in the above values are large, the differences in the values measured at different epochs are significant.

From our timing observations, we have obtained the period of the pulsar as 0.426676786723(4) secs and the period derivative is $1.2 \pm 0.2 \times10^{-18}$ ss^{-1} at the epoch JD

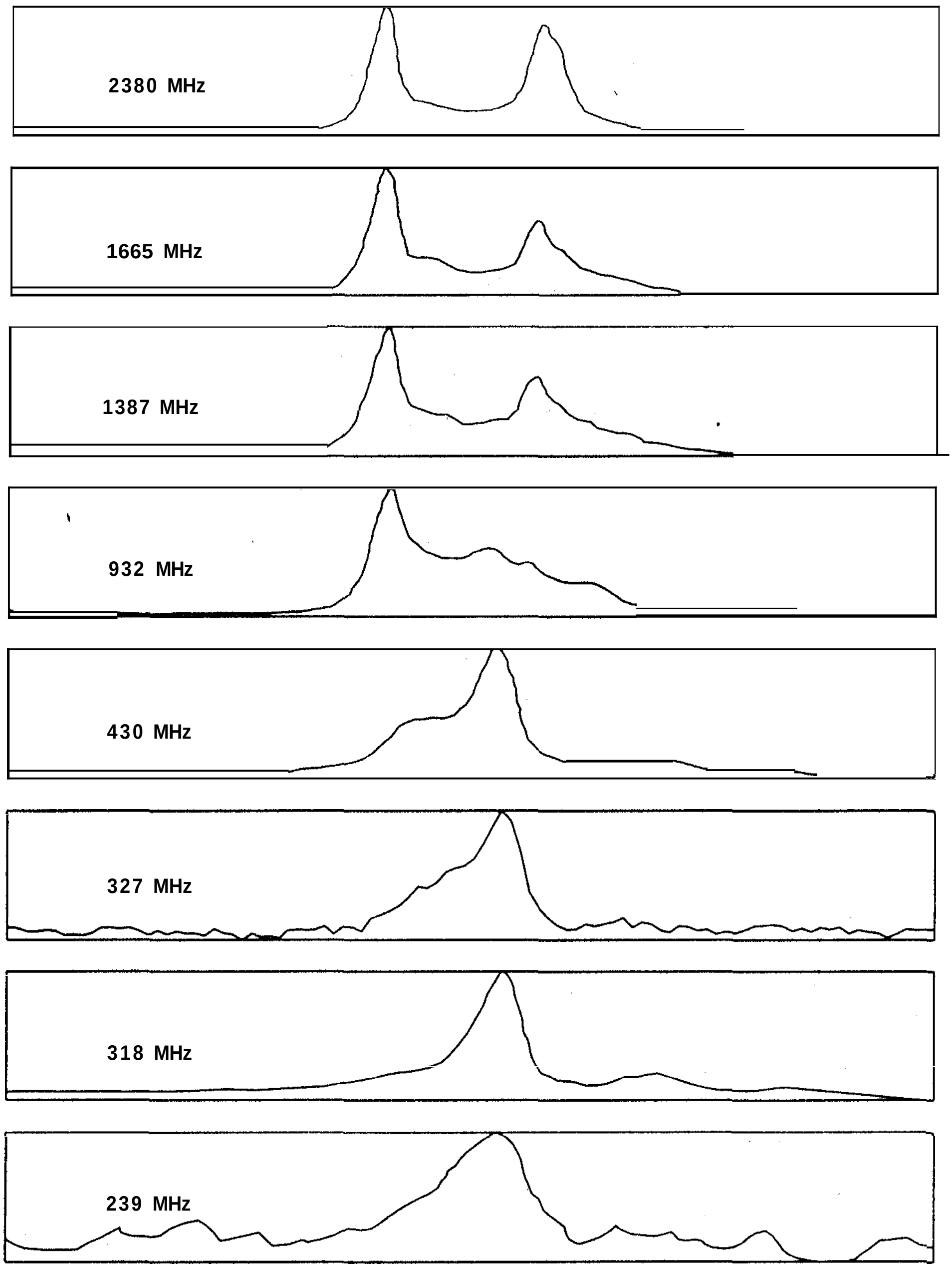

Figure 4.16: The pulse profile of PSR B1952+29 at various frequencies. Our measurement is at 327 MHz. All the profile spans correspond to quarter of the period centered around the pulse window.

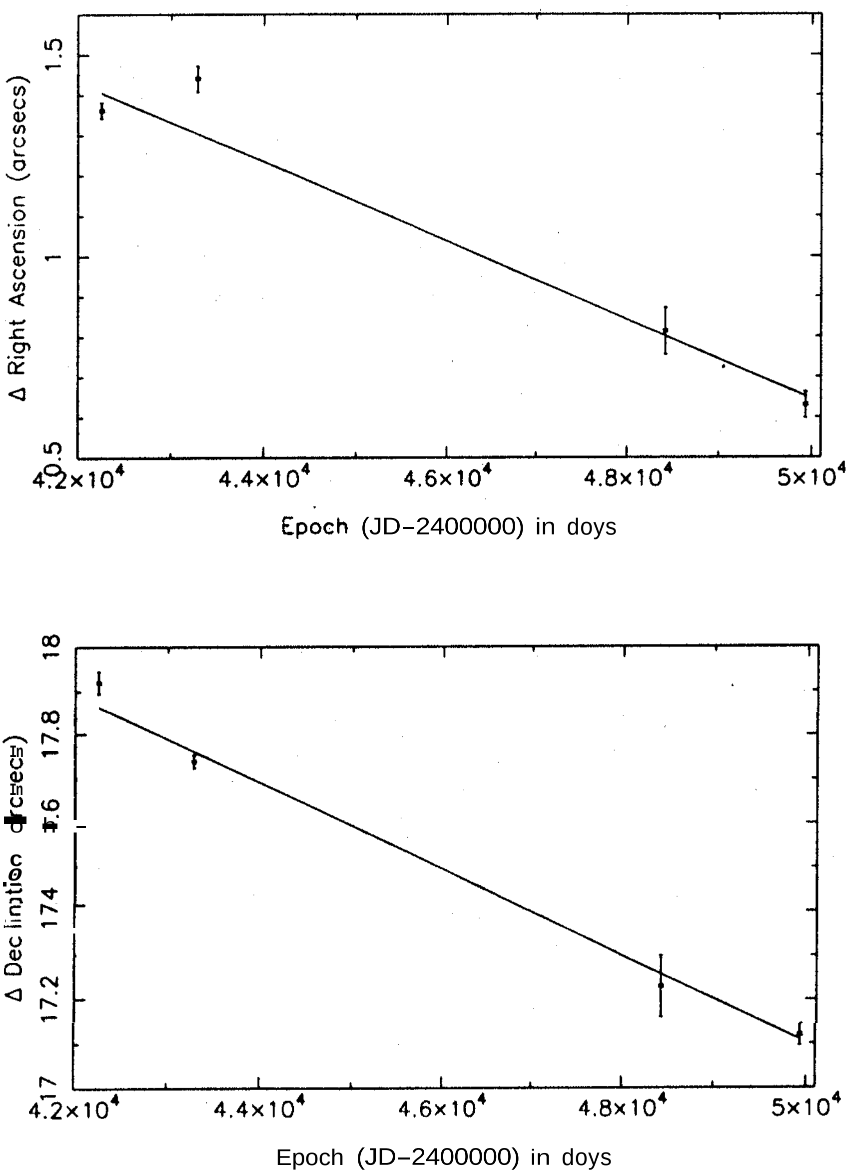

Figure 4.17: Least-square fits for proper motion in RA & Dec. The total time span is ~21 years. A RA & A Dec are with respect to HA = 19^h 54^m $22^s.5$ and Dec = +29° 23'.

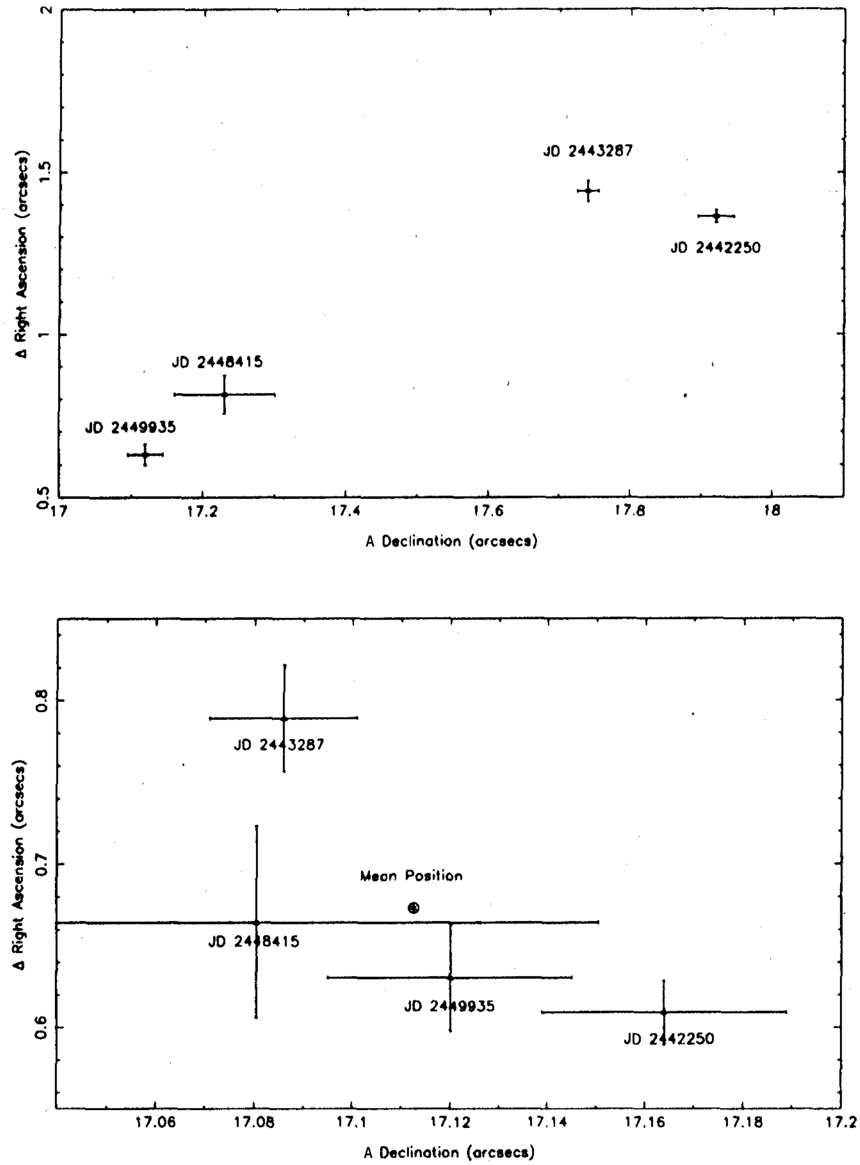

Figure *4.18:* **The position of the pulsar at various epochs. In the bottom figure, the position of the pulsar is shown after removing the proper motion with filled triangles and the mean position is also marked for the epoch JD** *2449935.* **Δ RA & Δ Dec are with respect to RA = $19^h\ 54^m\ 22^s.5$ and Dec = $+29°\ 23'$.**

Epoch (JD)	RA (J2000)	DEC (J2000)	Reference
2442250.0	19 54 22.599(3)	+29 23 17.92(5)	Mansfield & Rankin 1977
2443287.0	19 54 22.605(5)	+29 23 17.74(3)	Lyne et al. 1982
2448415.0	19 54 22.557(9)	+29 23 17.23(14)	Arzoumanian et al. 1994
2449935.4	19 54 22.543(5)	+29 23 17.12(5)	Our measurement

Table 4.4: Position of PSR B1952+29 at various epochs

2449935. We have also tried to determine the position of this pulsar at the epoch of JD 2449935 using our timing observations over one and a half years. Position of this pulsar at various epochs (our measurements and from earlier literature) are listed in Table 4.4. From these values of the position, we have estimated the proper motion of this pulsar to be

$$\mu_\alpha = -36 \pm 3.4 \quad \text{mas/yr}; \tag{4.13}$$

$$\mu_\delta = -36 \pm 2.9 \quad \text{mas/yr} \tag{4.14}$$

(see fig.(4.17)), which is quite different from any of the three values given by other groups as mentioned earlier. The magnitude of the proper motion is

$$\mu = 50 \pm 4.2 \quad \text{mas/yr} \tag{4.15}$$

which gives a transverse velocity of about

$$v_{\text{pm}} = 37 \pm 8 \quad \text{km/sec} \tag{4.16}$$

assuming the pulsar to be located at a distance of 160 pc (Prentice & ter Haar 1969). This distance, obtained by considering the electron density in the solar neighbourhood to be –0.05 cm^{-3}, is quite different from the Catalogue value of 420 pc. For local population, we believe the estimate by Prentice & ter Haar than Taylor-Cordes electron density model because it takes into account of the local ionised hydrogen regions properly. The mean position of the pulsar at the epoch JD 2449935 is estimated to be $\alpha = 19^h54^m22^s.546$ and $\delta = 29°23'17".13$ (see fig 4.18).

Shklovsky(1970) pointed out that any transverse velocity will act to increase the observed spindown rate $\dot{P}_{\text{pm}}$ by an amount $v_{\text{pm}}^2 P/cr$, where r is the distance to the object and c is the speed of light. This quantity is quite negligible relative to the observed values of $\dot{P}$ for many pulsars, but for those pulsars whose period derivative is as low as in the present case, the effect is of crucial importance. Then the observed period derivative is, $\dot{P}_{\text{obs}} = \dot{P}_{\text{o}} + \dot{P}_{\text{pm}}$, where $\dot{P}_{\text{o}}$ is the intrinsic period derivative. This quantity $\dot{P}_{\text{pm}}$ is found to have $0.42 \times 10^{-18} \pm 0.11 \times 10^{-18}$ ss^{-1} and for the catalogue distance of 420 pc this value turns out to be 1.1×10^{-18} ss^{-1}. Subtracting the former $\dot{P}_{\text{pm}}$ value from the observed period derivative at the epoch JD 2449935.0 gives an value of $(0.78 \pm 0.34) \times 10^{-18}$ ss^{-1}, implying that the pulsar is not spinning up, contrary to the conclusion by Marisfield &

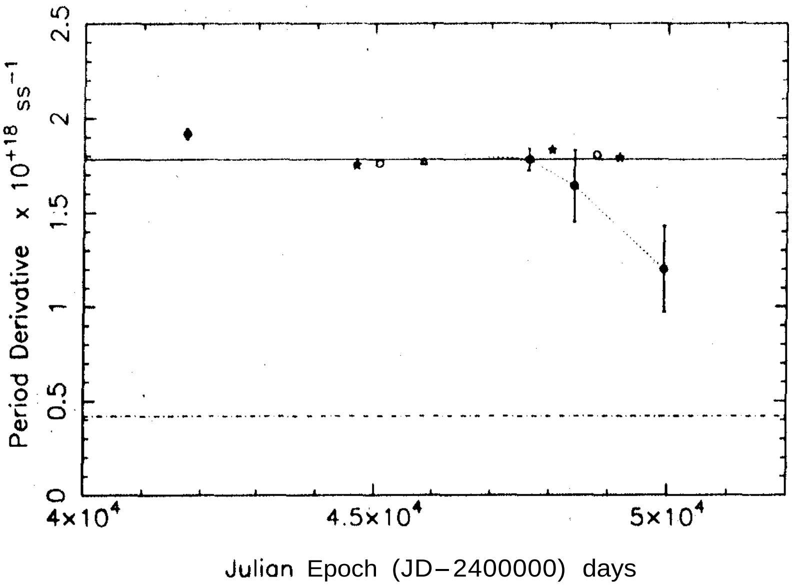

Figure 4.19: Observed Period derivative as a function of epoch. Circled plus are the observed $\dot{P}$s which are connected by dots. The stars are the estimated $\dot{P}$s from the adjacent epoch periods while the circles are from the alternate epoch periods and the triangle from the extreme epoch periods. The solid line represents the average value of the estimated $\dot{P}$'s. The dot-dashed line corresponds to the contribution from the gross proper motion that we have measured to the observed period derivative.

Rankin (1977) that the intrinsic period derivative is negative basically because the proper motion estimated by them was very high.

We find another puzzling thing, that is, when we compare our P estimate with earlier similar estimates, the apparent period derivative is reducing systematically as shown in fig.(4.19). These period derivatives are not corrected for the Shklovsky effect. This decrease appears significant unless the error bars are grossly underestimated. Variation of P can be expected in the following three cases.

- Change in P can be interpreted in terms of change in surface magnetic field strength. Jahan Miri (1996) has discussed the possibilities of such change in field strength in cases where the pulsar has/had binary companion. However, the apparent rate of change in $\dot{P}$ observed over $\sim$ 20 years is too rapid to be accounted for by such a change related to the surface magnetic field of the star.

- Apparent variation in P is also observed in a case of a'glitching pulsar during the recovery from a glitch. But the timescale in such a case is of the order of an year or so which is much less compared to the timescale over which the variation of period derivative observed. Moreover, this pulsar is, in any case, relatively old.

- A more likely and interesting possibility would be that this pulsar being a member of a binary system. It may be possible to understand the apparent change in the $\dot{P}$ due to the Shlovsky effect. We have given some constraints on a possible binary orbit with this observed P variation.

Given the fact that this possible system has not been identified as a binary through standard signatures in the timing residuals, we prefer to assume that the plane of the binary orbit is in close inclination with the plane of the sky (perpendicular to our line of sight), i.e. the binary orbit is face on. If this system did not have a gross proper motion, while the pulsar moved only in a circular (face on) orbit, then this orbital motion would give only a constant and not a varying contribution in the apparent P whereas if the orbit were an elliptical orbit, P would vary depending upon the transverse velocity at any instant. Far simplicity, we have considered the case of a *face on circular* orbit, in addition to the proper motion of the system.

At any instant, the transverse velocity due to the gross proper motion and the orbital motion can be written as

$$v_{\perp}(t) = \sqrt{[|v_{\rm pm}| + |v_{\rm orb}|\cos(\theta(t) - \theta_{\rm pm})]^2 + [|v_{\rm orb}|\sin(\theta(t) - \theta_{\rm pm})]^2} \tag{4.17}$$

and hence the observed period derivative is

$$\dot{P}_{\rm obs} = \dot{P}_{\rm o} + \dot{P}_{\rm pm} + \dot{P}_{\rm orb} + \frac{2v_{\rm pm}v_{\rm orb}P}{cr}\cos(\theta(t) - \theta_{\rm pm}) \tag{4.18}$$

where $v_{\rm pm}$ is the velocity corresponding to the gross proper motion, $v_{\rm orb}$ is the orbital velocity anti $\theta_{\rm pm}$ is the angle of the proper motion direction. The equation (4.18) shows that the variation in P is due to the fourth term corresponding to a maximum swing $\propto 4v_{\rm pm}v_{\rm orb}$ and this variation is about the mean $\dot{P} = \dot{P}_{\rm o} + \dot{P}_{\rm pm} + \dot{P}_{\rm orb}$. But all the information that we have, to get some constraints on the orbital parameters are the values of observed period and period derivative at four epochs. We consider two distinct possibilities for the "true" timescale of the variation. One where the orbital period being much longer compared to the total time span of these data and another where many orbital cycles have occurred within the time span and in each observation one has sampled an arbitrary phase of the orbit. It is possible to distinguish the above two cases as follows. If we calculate the period derivative by finding the difference in the apparent periods at two different epochs and dividing it by the time interval, this estimated value of P should always lie somewhere in between the observed $\dot{P}$'s at the two epochs, if the former was true. But if the calculated P lies outside the two $\dot{P}_{\rm obs}$, this may indicate that the orbital period is smaller than the time span that one is looking at. The $\dot{P}$'s calculated this way for all possible combinations of epochs are plotted in fig(4.19) using different symbols (refer to the caption for the details). What we find is that 'all' the $\dot{P}$'s thus calculated lie in a small range compared to the large variation seen over the 20 year span. This is possible only if the orbital period is much smaller than the time spans considered for the calculation of the period derivative from the observed periods. The estimated P would lie within an envelop of sinc function (see fig 4.20), with the exact location depending upon the number

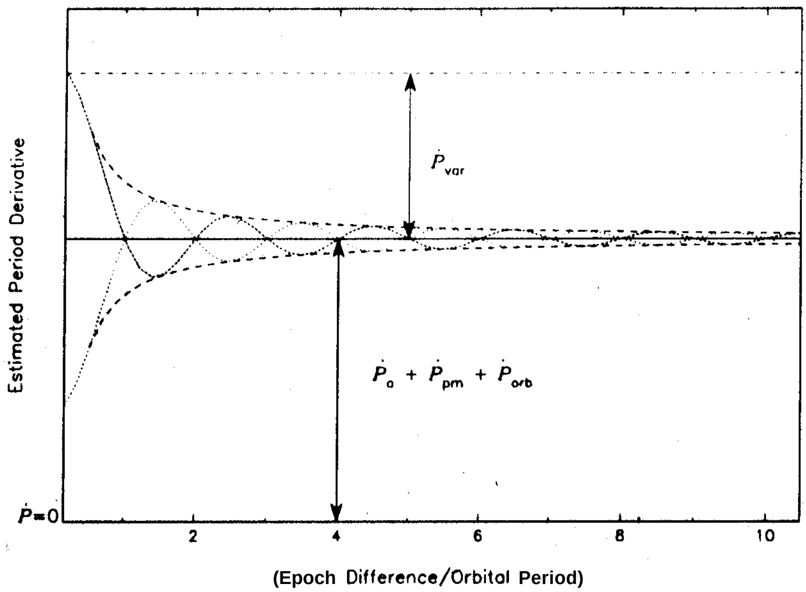

Figure 4.20: Variation of the estimated period derivative from the period at different epochs follows a **sinc** function. Here $\dot{P}_{\rm var}$ stands for the expression $2v_{\rm pm}v_{\rm orb}P/cr$.

---

of orbital periods within the time span At between the two epochs and the phase of the orbit at the two epochs considered. The maximum variation in $\dot{P}$ calculated this way will reduce as $1/\Delta t$, if the orbital period is smaller than At.

The average value of such $\dot{P}$s is 1.78 x 10^{-18}ss^{-1} and might well correspond to the value of $\dot{P}_{\rm o}+\dot{P}_{\rm pm}+\dot{P}_{\rm orb}$. The difference between this mean value and the period derivative from our measurement would give a lower limit to the peak variation expected due to the orbital motion, and is estimated to be 0.58 x 10^{-18}ss^{-1}. This would give us a lower limit for orbital velocity, $|v_{\rm orb,min}| \simeq 23$ km/s using the fourth term of the equation (4.18), implying in turn that $\dot{P}_{\rm orb,min} = 0.16$ x 10^{-18}ss^{-1}. Using the $\dot{P}_{\rm orb,min}$ and $\dot{P}_{\rm pm}$, we estimate an upper limit to the intrinsic period derivative to be 1.2 x 10^{-18}ss^{-1}. Also if one uses 2 x 10^{-18}ss^{-1} as an upper limit for the mean P and assumes that the intrinsic $\dot{P}$ is zero, we will get $\dot{P}_{\rm orb} < 1.58 \times 10^{-18}$ss^{-1} implying $|v_{\rm orb}| < 73$ km/s. As the maximum orbital period ($P_{\rm orb,max}$), we use the shortest difference between two measurement epochs. Using the $P_{\rm orb,max}$ ($\sim$ 800 days) and $|v_{\rm orb,max}| = 73$ km/s, we estimate the possible size of the orbit as 5.2 AU.

Another intriguing thing is that this pulsar is one among the few 'active' pulsars which lie below the "death line", where the death line is defined by the following equation (Ruderman & Sutherland 1975)

$$\frac{B_{12}}{P^2} = 0.17 \tag{4.19}$$

where B_{12} is the magnetic field in units of 10^{12} Gauss and P is the period of the pulsar in seconds. Apparent variation in the observed $\dot{P}$ can be observed in the $\log(\dot{P})$–$\log(P)$

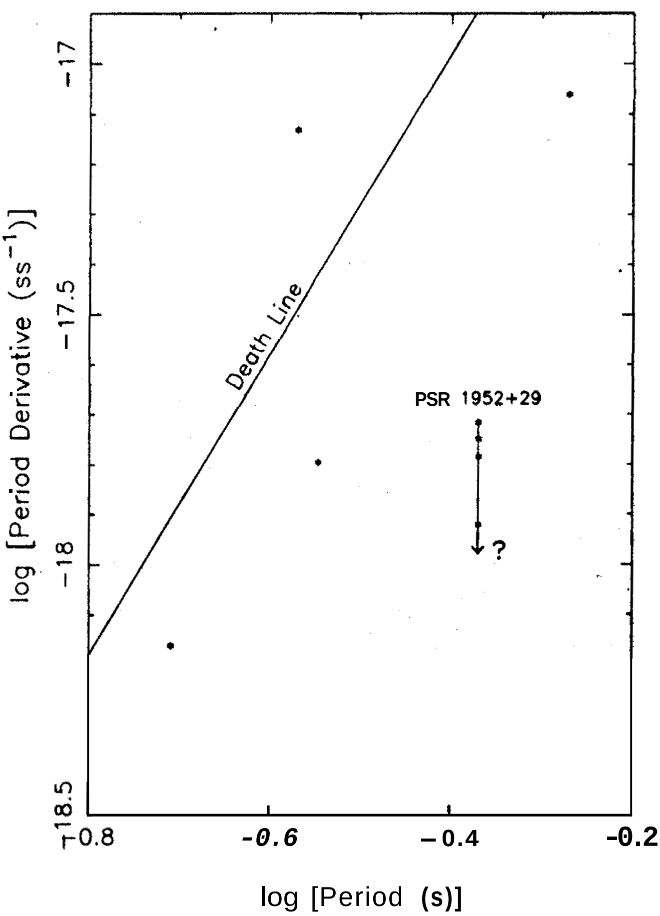

Figure 4.21: Motion of the pulsar in the log($\dot{P}$)–log(P) diagram. PSR 1952+29 is below the death line and the apparent change in P is marked by an arrow.

diagram (fig 4.21) as a vertical motion downwards. Clearly this pulsar has much to be explained in terms of its motion and apparent rate of slowing down. We plan to monitor this pulsar for the next few years as well as try to see if more measurements at earlier epochs would be available, as at present there are too few data to attempt any elaborate modelling of the "true" system.

Summary of the Results

- Integrated profiles for 16 pulsars at 327 MHz are obtained. Classification of these profiles is attempted by measuring the pulse width and comparing them with the expected minimum width for the core component. Most of the measured widths were greater than the expected minimum width for the core component while PSR 52347-0612 shows a clear conal double profile and one pulsar (51034-3224) shows multiple components.

- Using the observations spanning over a year, we have obtained period derivatives for the first time and refined the estimates of the periods for all the 16 pulsars in our final sample. We also report the improved positions for all cases where the earlier position estimates had uncertainty of a few arcminutes. Out of the 16 pulsars 12 fall in the main island of pulsars in the $\log(P)$-$\log(\dot{P})$ diagram, while four lie in the less dense area. There .is a possibility that some of these pulsars are members of binary systems. Future observations would be able to test this possibility.

- We have reported the scattering delay measurements for 10 pulsars at 327 MHz. One of these, PSR 51045-3033, shows excessive scatter broadening that is two orders of magnitude larger than that expected from its dispersion measure. We associate the scatterer tentatively with the 'possibly extended' region of the Gum Nebula.

- We have presented a brief account of re-analysis of pulsar current and birth rate after including our sample of pulsars and the latest Parkes Survey which increased the sample set from 322 to 443. We find the pulsar birth rate to be one in 100 $\pm$ 25 years, which is consistent with the earlier values such as one in 75 $\pm$ 15 years obtained by Deshpande et al. (1995) and one in 100 years derived by Narayan & Ostriker (1990). The birth rate of pulsars with magnetic fields in the range of $10.5 < \log B(\mathrm{in Gauss}) < 11.5$ appears to be roughly one in 10,000 years, which is lower than the earlier estimate.

- We have made some investigations on an interesting pulsar PSR 1952+29. We have estimated the proper motion of this pulsar to be 50 mas/yr, which is quite different from the values obtained by earlier groups. By subtracting the contribution of proper motion to the observed P, we find the intrinsic P is positive, contrary to the conclusion by Mansfield & Rankin (1977), who estimated the intrinsic $\dot{P}$ to be negative basically because their measured proper motion was very high. Also, we observe a systematic and significant reduction in the observed P over a span of ~ 20 years and argue that the observed variation can be understood better in terms of a possible orbital motion of the pulsar. So, based on the available data, we discuss the possibility of the pulsar having a binary companion. We estimate the upper limit to the intrinsic P to be 1.2×10^{-18} ss^{-1} and if the pulsar is in a binary the possible size of the orbit is 5.2 AU.